CHARACTERIZATION OF THE STANDARD IMAGING EXRADIN W2 SCINTILLATOR DETECTOR FOR SMALL FIELD DOSIMETRY

By

Austin M. Sloop

A THESIS

Presented to the Medical Physics Graduate Program
and the Oregon Health & Science University
School of Medicine
in partial fulfillment of
the requirements for the degree of

Master of Science

June 2021

Table of Contents

List of Figures

List of Tables

Acknowledgements:

i. I want to express my appreciation and gratitude to my mentor, Dr. Stephanie Junell, for her support and guidance on this project amid the uncertainties the pandemic offered. I appreciate your flexibility through the iterations of this project and for helping guide my focus. Also, thank you for your insight and advice on my professional development.

ii. I would like to thank my committee chair, Dr. Kyle Gallagher, for his input throughout the project, his professional advice, and for his time spent training me to use the tools of our field.

iii. I would like to thank Dr. Andrei Pugachev for his guidance and for encouraging precision and attention to detail in the academic setting and beyond.

iv. I would like to thank the greater OHSU radiation oncology department, for sharing data needed for this project and for always being open to questions and opportunities to engage across professional fields.

v. I would like to thank my family, for their love and support through this project, the pandemic, and the academic journey to this point. Also, special thanks to my partner Lynn for her encouragement, love, and support in all aspects of my life. You helped keep me grounded to what is important through my graduate degree.

vi. Lastly, I want to thank Dr. Kamesh Sankaran of Whitworth University. Your classes challenged me to strive for my academic best and taught me that education is not a solidary endeavor. I deeply appreciated your support through the challenges of my double undergrad, and your encouragement to “stay the course” has stuck with me through the years.

Abstract

Advanced external beam radiation therapy treatments such as intensity modulated radiation therapy and stereotactic radiosurgery are reliant on precise characterization of small radiation fields. There are numerous physical effects interplaying between the radiation field, the medium, and the detector that influence and challenge the accuracy of dosimetry in non-equilibrium environments. Standard Imaging's Exradin W2 scintillation detector was recently introduced to the field and aims to increase accuracy of small field measurements. The performance of the W2 was measured and compared to compared to the PTW microDiamond, another common detector suitable for small-field dosimetry. Small-field output factors, anisotropy, and performance in beam scanning were evaluated. Output factors were found to be similar to the microDiamond for field sizes larger than 1x1cm^2, but the W2 showed an increased response at the smallest field size. The detector displays considerable anisotropic behavior outside of its radial dimension with sensitivity varying up to 30%. The W2-1x1 and W2-1x3 models of the detector performed similarly when making lateral measurements of beam profiles, and there is evidence to suggest the W2 may characterize penumbra measurements differently than the microDiamond. Cherenkov contamination in the fiber optics can be managed but differences in fiber irradiation should be minimized throughout measurements. The W2 detector was determined to be a viable detector for small-field dosimetry if anisotropy is accounted for.

Introduction

The Exradin® W2 Scintillator detector (Standard Imaging, Middleton, Wisconsin) is a recently released detector designed to excel in small-field situations. At the time of writing, there has yet to be any published independent validation of its performance and the only published work lacks information about any angular dependance (Galavis, 2019). The purpose of this project was to characterize the dose linearity, dose rate linearity, and anisotropy of the W2, and compare output factor and beam profile measurements to another detector commonly used for small-field dosimetry. Measurements of the detector dose response, output factors, and beam profiles were measured in water and angular dependance was investigated using a LUCY® 3D QA Phantom (Standard Imaging, Middleton, Wisconsin). Selected characteristics were compared to the microDiamond detector (PTW, Freiberg, Germany).

1.1 Small Field Dosimetry

The reference dosimetry of high energy photon beams in the United States is rooted in the American Association of Physicists in Medicine's Task Group (TG) 51 report (Almond, 1999) and its addendum articles (McEwen, 2014). This Code of Practice defines reference conditions and traceable measurement devices to standardize the calibration of Linear Accelerators (Linac). Advances in treatment planning systems, machine technology, and image guidance have increased the number of radiotherapy treatments that rely on small radiation fields through the delivery. Stereotactic radiosurgery and intensity modulated radiation therapy treatments rely on small beams to precisely deliver dose to a target while minimizing radiation doses to healthy tissues. These small fields

pose many physical challenges that make precise measurements or characterizations of the beams difficult. Errors in the measurements that characterize the beam models used in the treatment planning systems to calculate dose could result in severe patient harm if the actual output differs from what the planning system calculated.

The International Atomic Energy Agency (IAEA) and the American Association of Physicists in Medicine collaborated to produce a standardized code of practice for measuring small radiation fields that was recently published in 2018. They define a small field as any external photon beam under at least one of the following conditions: a) There is a loss of charged particle equilibrium on the beam axis; b) there is partial occlusion of the primary photon source by the collimating devices; or c) the detector dimensions are similar or larger than the size of the beam being measured (IAEA, 2017).

Charged particle equilibrium (CPE) describes the condition where, for a given volume, the fluence of ionizing charged particles entering that volume is the same as those exiting. This allows for an accurate measurement of dose deposited because it accounts for all the energy deposited along the ionization tracks on the assumption that any particle that carries excess energy out of the region is replaced by another entering. Under such conditions, the amount of energy ultimately absorbed is the same as the KERMA, or amount of kinetic energy transferred by primary interactions with the beam (Mcdermott, 2018). In a medium, there are typically two forms of equilibrium. Normal CPE and transient CPE. Charged particle equilibrium requires a constant radiation fluence to maintain, such as seen in the lateral direction from an ideal broad beam radiation field at a fixed depth in matter. When there is a reduction in that fluence due to attenuation

by matter, such as seen when evaluating a system along its depth axis, the equilibrium takes form as a proportional relationship between the dose and KERMA with a proportionality constant slightly greater than one. Dose is higher than KERMA because losses in fluence due to attenuation reduce the number of primary interactions with increasing depth, but upstream interactions can reach a deeper location and deposit energy. In the lateral dimension, when the average range of a secondary electron exceeds the half-field size of a beam, this equilibrium cannot be reached as there is no opportunity for this inward scatting to balance the outward scattering (Figure 1).

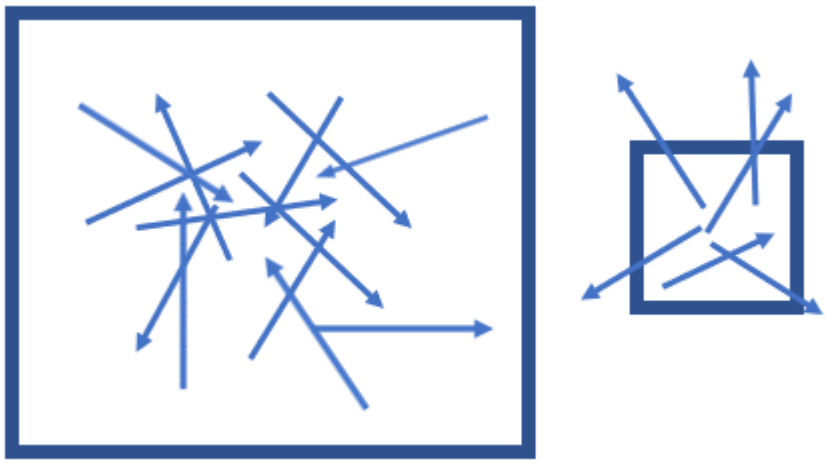

Figure 1. Example of loss of lateral charged particle equilibrium for small beams. When the field size is reduced below the average range of secondary electrons, there is a reduction of the inward scattering component leading to a violation of CPE and a reduction in the absorbed dose.

Li et al (Li, 1995) used Monte Carlo calculations to determine the field sizes at which this effect becomes significant and how much the absorbed dose can differ. Their results showed that the loss of lateral CPE will severely reduce the output for fields below 1cm, but the effect quickly diminishes for larger fields.

Partial occlusion of the source, as demonstrated in Figure 2, is a phenomenon resulting from the finite size of the transmission target. In a large field, there are three conditions a location can face with respect to the target. If the location does not have any line of sight to the source (completely blocked by collimating devices), then there will be no direct radiation to that point and only scatter will contribute to dose. In the central regions where a location has line-of-sight to the entire source, the full output can be delivered to that point. Gradients in this region tend to be gradual and small. Between these regions, where the source is partially occluded by one collimator, there will be a rapid reduction in falloff as less direct radiation can reach a point. This results in very steep gradients that contribute to the penumbra of the beam, or the region where the dose falls from 80% to 20%. Precise measurements in the penumbra region can be difficult as perturbations in location can result in a large difference in measured dose. In very small fields, it is possible that no location has a full line of sight to the entire x-ray producing region of the source and the overall output is a summation of two regions in the geometric penumbra. This will result in a very centrally peaked dose profile with steep gradients, as well as energy spectrum changes that can influence detector response as the MLC and jaw tips partially attenuate and harden the beam (IAEA, 2017) but there can be an

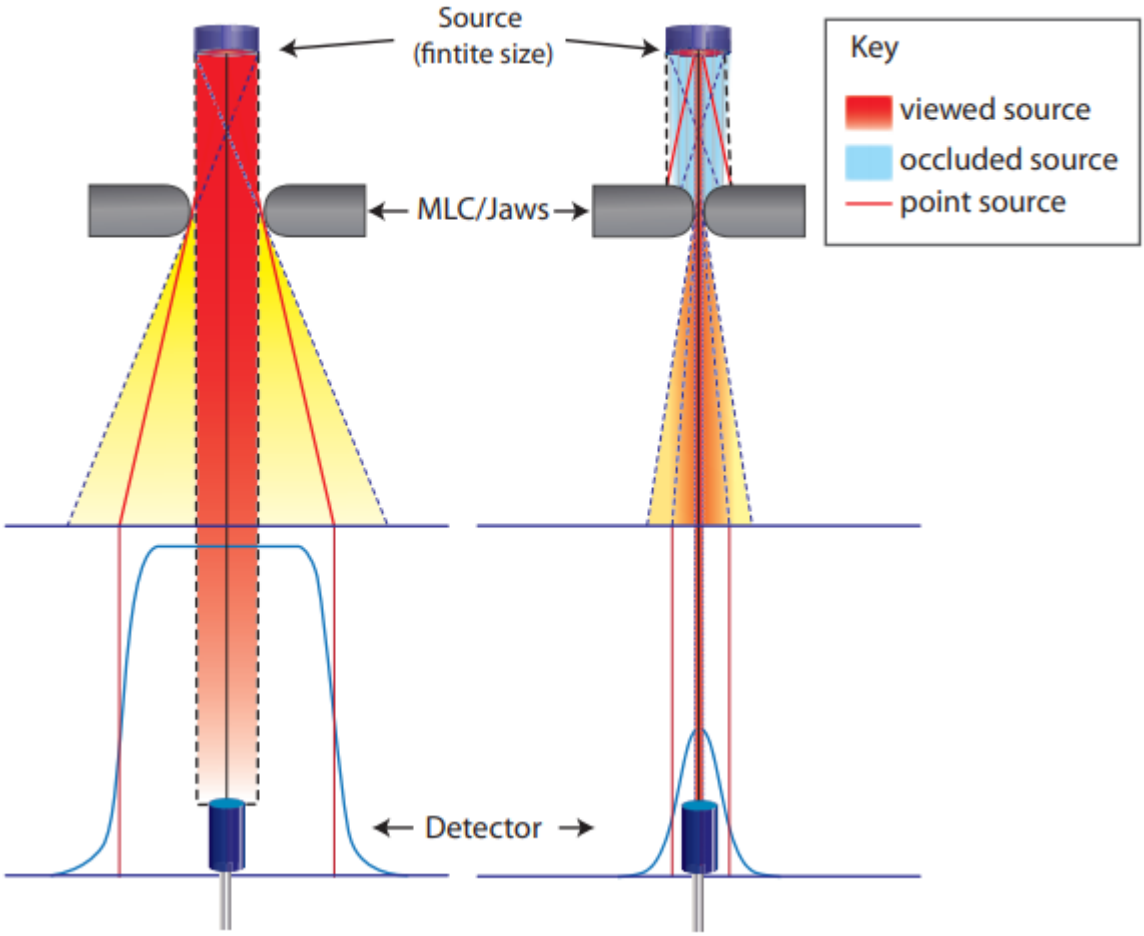

Figure 2. Source occlusion effect. In very small fields, the source can be partially blocked by the collimating elements leading to a significant reduction in output. The exact profile can be hard to measure if the detector volume is large in comparison as partial volume averaging will smooth out the profile. From Dosimetry for Small and Nonstandard Fields (Junell, 2013). Reproduced with permission.

increase in low energy scatter components (Junell, 2013). It is an important note that spectrum changes can affect a detectors ability to produce an accurate measurement as non-water equivalent detectors that have high Z components can exhibit a higher response to low energy photons. Modern Linacs incorporate small targets that prevent

bilateral occlusion of the beam down to field sizes smaller than those for which CPE is lost (Palmans, 2018).

While the former two conditions are dependent on characteristics of the machine and the beam, the detector size can also influence the reliability of a measurement. Radiation detectors operate under a volume average effect, where the output signal is an average response of the dose across the entire active volume. If the radiation field crossing the detector is inhomogeneous, which can happen when measuring very small fields, this can result in an erroneous measurement that is missing information about a small hot-spot or result in increased uncertainty about the dose at an exact location. This ultimately will result in underestimating the dose in a peaked region, potentially overestimating the dose just outside a field, and can smooth measurements of the penumbra region making the falloff appear more gradual (Wuerfel, 2013). Accurate penumbra characterization is extremely important for EBRT techniques that modulate the beam down to numerous beamlets, such as is the case in intensity modulated radiation therapy treatments. When all the overlapping regions are added in total, a significant amount of the dose delivered will come from penumbra regions (Das, 2008).

When measuring output factors for small field sizes, losses of CPE, geometric source occlusion, spectrum changes, and partial volume averaging will all influence the accuracy of the measurement which can result in an incorrect value if not accounted for. IAEA TRS-483 (TRS-483) reports the correction factors for numerous detectors based on measurement and MC simulation (IAEA, 2017). Small detectors that limit partial volume

averaging and limit perturbation of the local radiation fluence have correction factors near unity.

The detector itself can also affect the radiation fluence locally if its material properties differ from the surrounding medium. The disjunction of a non-water equivalent material in a water or water-like medium such as tissue can perturb the electron equilibrium and cause violation of the Bragg-Grey cavity theory conditions (Palmans, 2018). This can result in an incorrect measurement in areas with a steep gradient, as well as detrimentally influence the measurement itself as local scatter is enhanced or reduced depending on the material properties.

1.2 Overview of Common Detector technologies

There are numerous detector designs commercially available for use in a clinical setting, each having advantages or shortcomings in certain situations. TRS-483 (IAEA, 2017) specifies certain characteristics that are desirable for small field dosimetry, but since a single detector is not going to excel in every category, one should select the detector best suited for the measurement conditions. Ideal traits were listed as <0.1% deviation in consistency or accuracy for: a) absolute dose measured across multiple readings; b) absolute dose measured across at least 3 orders of magnitude; c) dose rate linearity across the output range of the Linear Accelerator; d) dose per pulse linearity; e) energy independence across the energy range of the machine; f) size selected to keep volume corrections from measuring a small field below <5%; g) anisotropy for angles less than 60° from the detector axis should be <0.5%; h) a signal to noise (SNR) ratio of at least

3 orders of magnitude; and i) environmental stability (temperature, pressure, and humidity) within 0.3% (IAEA, pp. 64-65).

1.2.1 Ion Chambers

Ion chambers have been traditionally treated as the gold-standard radiotherapy for radiation measurement due to their inexpensive cost, ease of use, robustness, and consistency (Kumar, 2012). The active volume is a substance, normally air, and a pair of electrodes. They can be designed with parallel plate or cylindrical orientations. When radiation ionizes the gas, the ion and electron will migrate to the cathode and anode respectively when a voltage is applied. The magnitude of voltage will determine the operating characteristics of the chamber (Figure *3*) (Knoll, 2010). Measurements in clinical radiation therapy are made when operating in the ionization region as the measurement is stable even under small bias voltage fluctuations. Increased in voltage at these levels will not result in multiplication and a decrease would not prevent all charges from being collected.

Higher voltages can eventually accelerate the electron to high enough energies to ionize additional gas molecules, causing an avalanche reaction that increases the charge collected. If the chamber does not saturate, the signal can be proportional to the initial ionization. Under these conditions, the signal is extremely sensitive to fluctuations in the bias voltage, requiring a stable supply. Eventually, as the bias is increased, the avalanche will produce enough ionization that the resulting space charge will disrupt the electric field enough to stop further multiplication. Geiger-Mueller detectors operate in this

region; the output signal for any initial ionization is large and consistent, leading to the high sensitivity desired in survey meters (Knoll, 2010).

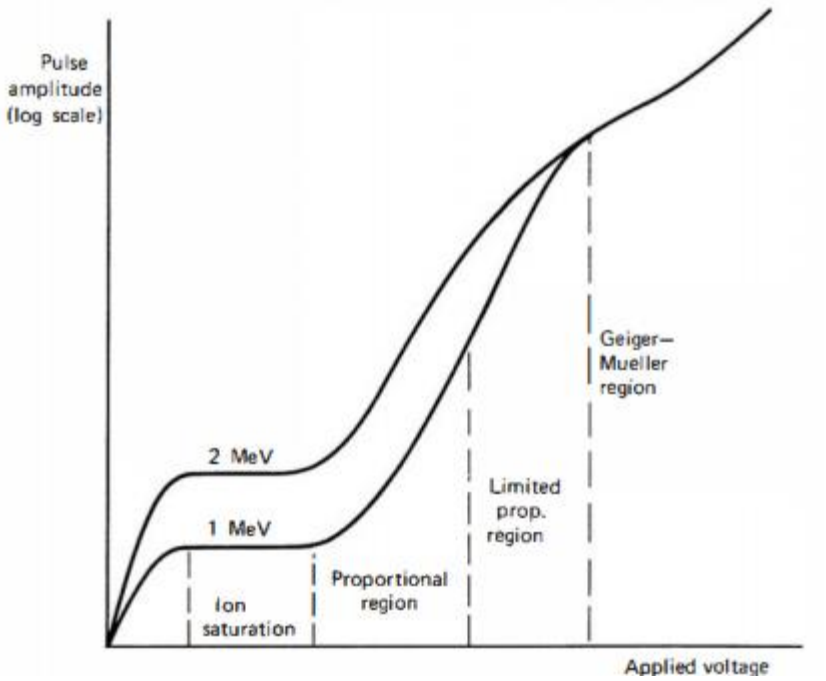

Figure 3. Signal-voltage response curve for an ionization chamber, highlighting the ion saturation, proportional, and G-M regions. Figure 6-2 From *(Knoll, 2010)*, Pending Permission.

Ion chambers require a large volume to produce a measurable signal, especially when a low-density medium such as air is used. Current chamber available on the market range from the standard farmer chamber (620mm^3) down to the PinPoint 3D (PTW, Freiberg, Germany) with an active volume of 16mm^3 or the Exradin A16 (Standard Imaging, Middleton, Wisconsin) with a volume of 7mm^3. The partial volume effect significantly reduces the accuracy of measurement in small fields or regions with a steep gradient. There are chambers available with small active volumes, but they can suffer

from poor SNR due to the low signal produced. These chambers tend to have stable energy responses and can measure a wide range of dose rates. When used for small field dosimetry, numerous correction factors are often needed to correct for the geometric effects, partial volume effects, and lack of CPE noted earlier (IAEA, 2017).

1.2.2 Semiconductor Diodes

Semiconductors are materials with a small band gap between the valence and conduction electrons that will pass current under certain conditions. Typical materials seen in dosimetric detectors are silicon or synthetic diamond that are doped with impurities to produce an imbalance of electron densities in different regions. At the border of the N side (increased electron density) and the P side (decreased electron density/increased hole density), a small electric field is induced as charges/holes are pulled to their respective counterpart. This area is known as the depletion region. When radiation passes through the material, an electron is excited into the conduction band leaving a hole in the valence band. Under the electric field induced in the depletion region, the charge/hole will migrate to regain equilibrium and that signal can be measured. Since the bandgap of these materials is much lower than the ionization threshold of air (as low as 3eV vs ~30eV), more charges are produced for a given amount of energy interacting in the active volume increasing the sensitivity and signal level (Knoll, 2010). This, in combination with a high material density, means that a strong signal can be produced from a volume smaller than $0.2mm^3$ (IAEA, 2017). Semiconductors tend to exhibit significant anisotropy, and silicon-based diodes will overrespond at energies in the kV range due to a higher equivalent Z value compared to water or air. Energy response in the

MV range is typically flat and rapid movement of the charge-hole pairs allows for measurements at high dose rates with short dead times. Silicon diodes will show degradation over the course of exposure and can suffer from a temperature dependence (Knoll, 2010).

1.2.3 Radiographic and Radiochromic Films

Radiographic film is comprised of a base material that is coated with a radiosensitive emulsion layer, usually silver halide crystals. Ionizing radiation will knock loosely bound electrons off the silver halide where they will reduce positively charged ionic silver that is present in the emulsion, converting it to metallic silver. When exposed to a developer chemical, this metallic silver will act as a catalyst to reduce the remaining silver in the crystal while the crystals with ionic silver will wash off. A fixer is then applied to halt the reaction and then the remaining silver halide is washed. The reduced crystals remaining are dark in color and the optical density (OD) of the film can be scanned for analysis (Bushberg, 2011).

Radiochromic film consists of a base layer coated in a polymer or crystal-containing emulsion layer. Gafchromic® film is one of the most widely used self-developing films in the clinical setting. When radiation interacts with the coating, the structural characteristics of the molecules will change its optical properties (i.e., color, or other absorptive characteristics), changing the optical density in real time. (Pierluigi, 2019)

The change in optical density of radiographic film is proportional to the log of the dose absorbed in the material, but the response of radiochromic films is more complex

and require calibration measurements for each batch that can differ depending on the scanning procedure (Borca, 2013). The calibration required for each batch of film is done by exposing small sections of the film to increasing dose levels and measuring the resulting OD or other optical properties. Films can suffer from a narrow dynamic range and typically require significant exposure, and radiographic film is sensitive to the exposure time under the developing chemicals (Bushberg, 2011). As an analog medium, film has the highest spatial resolution among currently used detectors.

1.2.4 Scintillation Detectors

The core operational principle behind a scintillation detector is that the material will emit visible light photons when exposed to ionizing radiation. They come in organic and inorganic varieties that have different properties that benefit certain applications. Liquid or plastic organic scintillators have a fast response time and can be made to be water equivalent but suffer from a low sensitivity. Inorganic scintillators, such as NaI, have a high light yield but the high Z results in an overresponse at low energies. Both will emit light at a longer wavelength that the material is transparent to, but the mechanism differs. For organic scintillators, a molecular electron is excited to a higher energy band when the radiation deposits energy into the material. If the electron is in the singlet state, it will promptly fluoresce. In the triplet state, the phosphorescence may be delayed on the order of milliseconds. In inorganic scintillators, the material is arranged in a crystalline structure with a large bandgap between the valence and conductions bands. The crystal is doped with a material to serve as an activator, providing a mediary energy state in the forbidden region between the valence and conduction band. When an electron is excited

to the conduction band, the positive hole will migrate to the activator ionizing it. An electron in the conduction band will drop down to the energy level of that ionized activator, and then reduce to the ground state releasing the energy difference as a photon. The energy level can be tuned to adjust the wavelength of the resulting light (Knoll, 2010).

For both organic and inorganic scintillators, the light produced is detected by a photodiode or photomultiplier tube that produces a current proportional to the incident light. If the electrical device is not abutted directly to the scintillator, some form of light guide is used to couple to the scintillator (Knoll, 2010). Acrylic is a common water equivalent compound used, but glass fibers or hollow lightguides are used as well (Galavis, 2019).

1.3 Cherenkov Radiation

While the speed of light in a vacuum, c, is the fundamental speed limit of the universe, the electromagnetic waves that are light will propagate at a slower speed when traveling through a medium. The ratio of the speed of light in a vacuum, c, to the propagation speed in a medium, denoted here as c_m, is the index of refraction N. The difference in wavefront velocity between materials is what causes light to bend or refract at material boundaries. It is possible for a high energy particle to enter a medium at a velocity higher than the speed of light in that medium. As a charged particle travels in the medium, it will interact with the medium exciting atomic electrons or ionizing atoms along the way. When a particle is traveling slower than c_m, the wave front of photons produced from characteristic x-rays and excitations returning to the ground state will outpace the

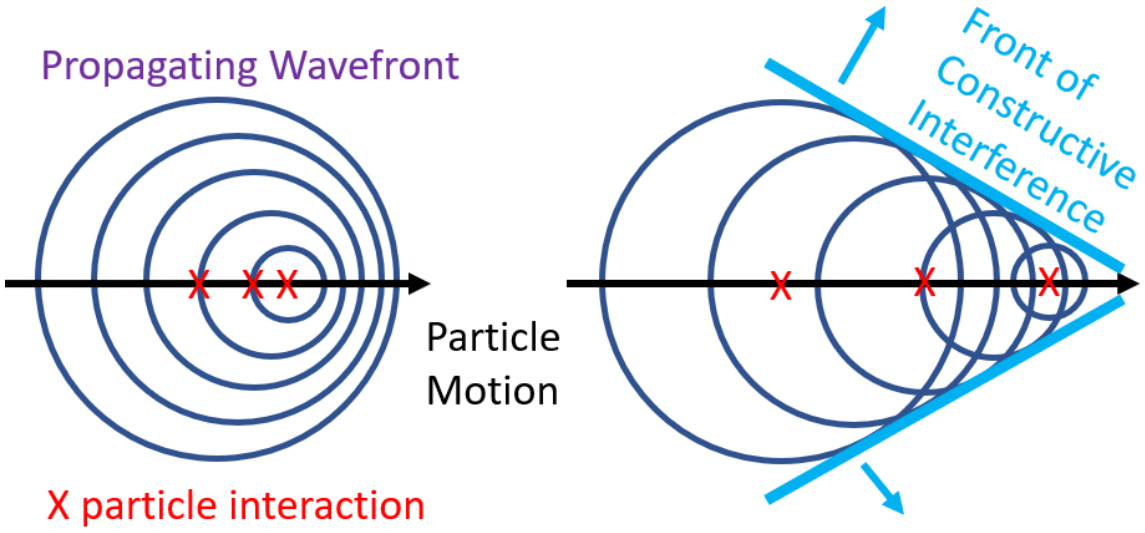

Figure 4 Diagram in interference mechanism behind Cherenkov Radiation. If a particle is traveling below the speed of light in the medium (left), the wavefronts from photons released through interactions will propagate faster than the particle. If the particle is moving faster than the wavefronts propagate (right), they will overlap resulting in constructive interference.

particle in transit. When the particle is traveling faster than *c/N*, the EM waves will begin to overlap and constructively interfere (Figure 4) (Alaeian, 2014). This is loosely analogous to the mechanical sound waves constructively overlapping when an object travels faster than the speed of sound in that material to produce a sonic boom. When EM waves constructively interfere, the energy of the photon increases and the wavelength shortens. The index of refraction is dependent on the wavelength, and as the wavelength approaches the x-ray range most materials' index of refraction will approach one. The result is that a photon's wavelength will shorten until it is able to transit the medium faster than the particle is traveling, stopping the constructive interference for that photon

as it travels out as Cherenkov Radiation (CR). Since the spectrum is produced through interference,

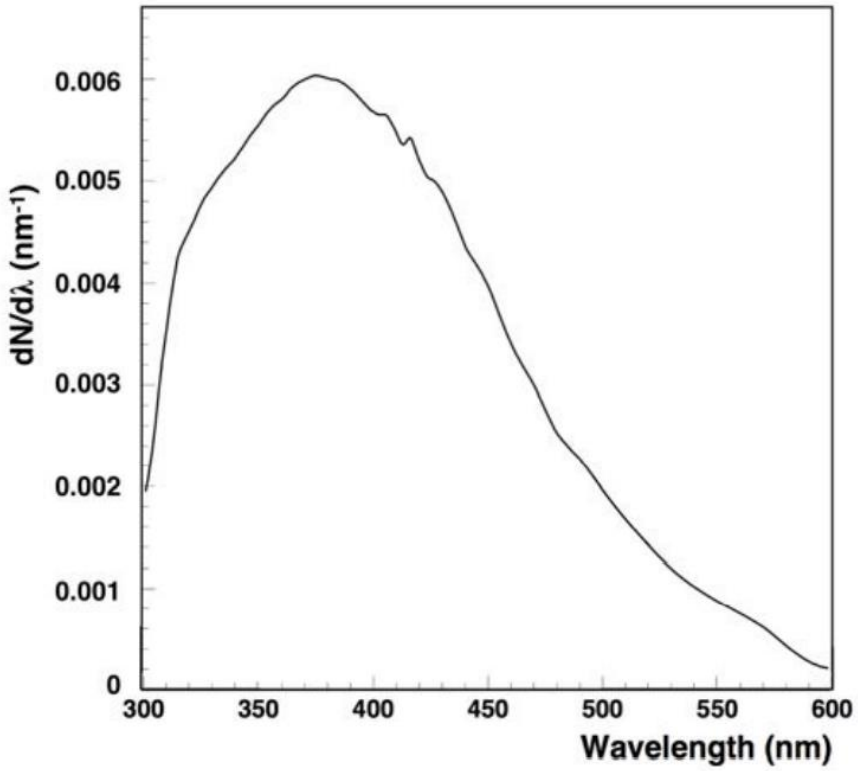

Figure 5. Cherenkov Radiation Spectrum measured in water. As the energy of the photons increase and the wavelength shortens, the refractive index will approach one near 300nm and the EM wave will propagate faster than the ionizing particle. This spectrum gives CR its characteristic blue color. PhD Dissertation, University Autonomous, Madrid. 2017. Used with permission. (Fernandez, 2017)

the spectrum is continuous, peaking at about 420nm in water and falling off in proportion to $1/\lambda^2$ (Alaeian, 2014). An example of the spectrum measured in water (Fernandez, 2017) is shown in Figure 5. The traveling particle will continue to produce CR until it has slowed below c_m. Production of CR requires a charged particle, but secondary electrons set in motion by high energy photons will produce this effect if they have sufficient energy.

1.4 The Exradin W2-1x1 Detector System

The Exradin W2-1x1 scintillating detector contains a small, 1mm diameter by 1mm long cylindrical active volume that will scintillate when exposed to ionizing radiation. There is also a W2-1x3 fiber available that increases the length of the cylinder to 3mm to increase sensitivity. Because this detector was brought to market recently, there is sparse external validation of its performance outside of the work published by Galavis et al (Galavis, 2019) as it has yet to reach widespread use.

The active volume is comprised of a doped polystyrene compound that is supposed to be water equivalent and have a flat energy response. It uses an acrylic fiber optic cable sheathed in a light-tight coating to transport the scintillated light to the MAX SD optical detector and signal processing unit. The MAX SD processes the incoming light signals, applies corrections, and provides a web-interface for calibration and measurement readout. It contains a built-in high-precision current output that can be used to provide a signal to other electrometers if desired. Whenever a portion of fiber is near the beam, there is a chance for CR production to affect the precision of the measurement if the CR photons were counted by the photodiodes. To correct for this unwanted signal, the MAX SD follows a process similar to the spectral method outlined by Guillot (Guillot, 2011).

The correction and removal of the Cherenkov signal is accomplished by splitting the incoming light and filtering each half with a narrowband green and blue optical filter. Ideally, the filters are designed so the overall response after the photodiode for one channel aligns with the spectrum of light produced from the scintillation volume, and the

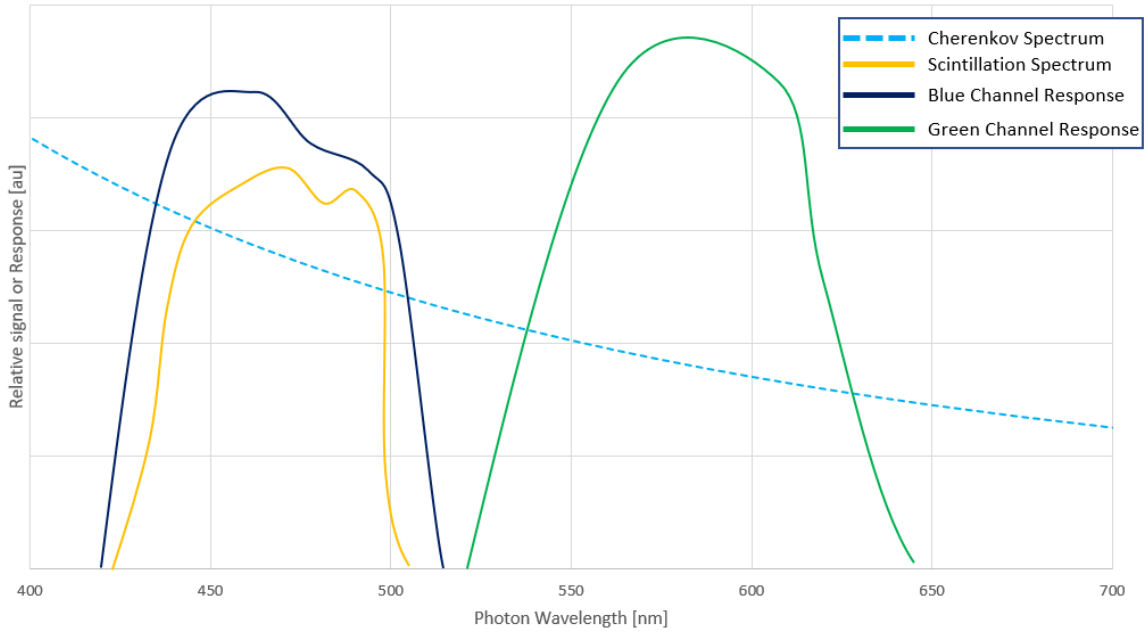

Figure 6. Illustration of the principles behind the spectral method of correcting for Cherenkov radiation developed by Galavis et al (Galavis, 2019). If one channel is well matched to the scintillation spectrum (blue) and the other is well isolated from it (green), the CR signal can be removed from the blue channel based on the amount of signal from the green channel.

other channel will have a minimal response to the scintillation light, as shown in (Figure 6). Since the Cherenkov spectrum produced in the acrylic can be characterized mathematically (L'Annuziata, 2016) or through measurement (Jang, 2013), it is possible to tune the optical filters and overall response between each channel to produce a linear, proportional response represented by the Cherenkov Light Ratio (CLR). The anticipated response to one channel is the CLR times the other channel. With these assumptions, it is possible to know how much signal is contamination that should be removed from one channel based on the signal from the other (Guillot, 2011). Standard Imaging deviates

slightly from Guillot's procedure in the selection of which filter handles CR and which handles the signal; the blue channel measures the combined Cherenkov and scintillation photon signals, and the green channel measures only the CR light (Standard Imaging, 2018). The corrected measurement signal from this device is calculated as: [$Blue - Green * CLR$] (Standard Imaging, 2018).

Determining the CLR requires collection of a few calibration points to measure each channel's response under specific beam configurations. Outside of a small scatter contribution, the CR light present in the fiber optics will be proportional to the amount of fiber optics in the beam. The system includes a bracket (Figure 7) that places controlled lengths of fiber in a 6x6cm^2 field. A fixed amount of radiation is delivered with the fiber centered at the depth of maximum dose (Dmax) and the response to each channel is recorded for the minimum and maximum fiber orientation. Calibration is necessary for each energy spectrum to be measured (Standard Imaging, 2018). Ideally, after calibration there should be no dependence on the amount of irradiated fiber and the CR should be corrected for (Guillot, 2011).

The microDiamond is commonly found in radiotherapy as a useful tool for point measurement or beam profile measurements due to its small size and relatively consistent radiation response. Some key characteristics relevant to small field measurements are compared to the W2 in Table 1.

	Exradin W2 1x1	**PTW microDiamond**
Detector Design	Polystyrene Scintillator	Diamond Diode
Active Volume	0.78mm^3	0.004mm^3
Active Area Dimensions	Cylinder, 1mm dia., 1mm thick	Cylinder, 2.2mm dia., 1µm thick
Coupling to measurement devices	Acrylic Optical Fiber	Triaxial Cable
Radiation damage effects	2% / kGy	0.05% / kGy (Khan, 2020)

Table 1. Comparison of the microDiamond and the W2. Information available on the manufacturer websites unless otherwise cited (Standard Imaging, 2021), (PTW Frieburg Germany, 2021).

Material and Methods

1.5 Device Calibration

The Exradin W2-1x1 Scintillation detector (SN: XAZ191936) was the focus of testing. The active volume is a 1 mm diameter by 1 mm long polystyrene based scintillator (volume of 8E-4 cm^3) coupled to a specialized electrometer, the MAX SD (SN: AE192740), by an acrylic fiber optic cable. The MAX SD handles all the signal processing for Cherenkov correction, provides a web interface for point measurement readout, and processes timed and triggered measurements. The MAX SD can provide a current output that is proportional to the detected signal for use in beam scanning.

The device also removes the contaminating Cherenkov light from the desired signal through calibration. The incoming light is split into two carefully selected spectral channels, Blue and Green, and the signals are compared under different set-ups to

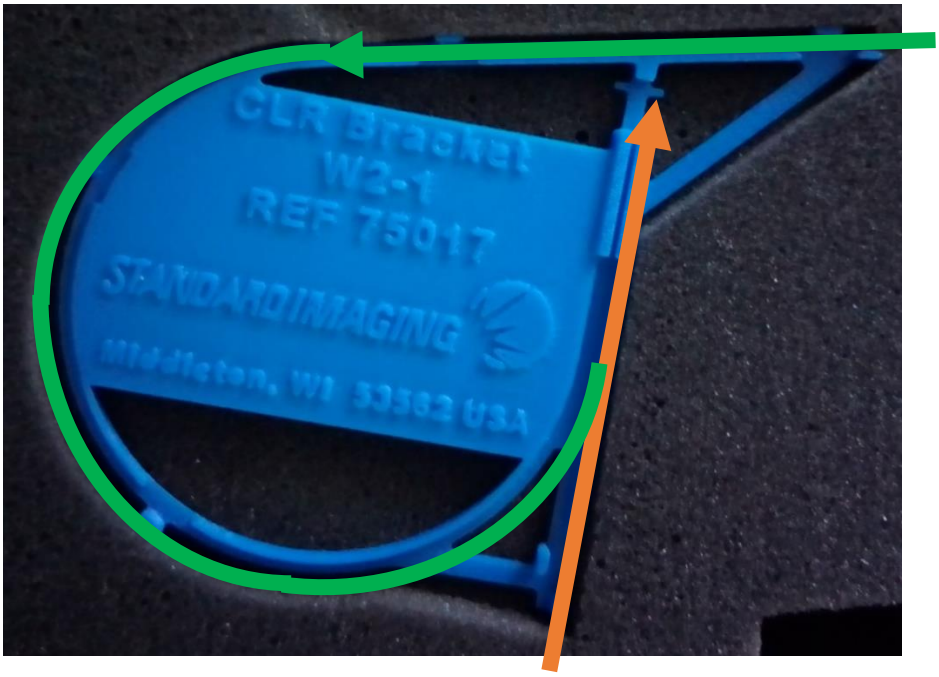

Figure 7. CLR Calibration Bracket for Small Fields. This holder will place a known quantity of fiber in the beam for two configurations required for CLR calibration: the short configuration (orange) and the long configuration (green). The cross marks the active region of the detector.

calculate the Cherenkov Light Ratio (CLR). The calibration procedure for small fields requires a delivery of a fixed amount of radiation to the fiber when it is placed in a specialized holder that places a known amount of fiber in the beam as shown in Figure 7. The blue and green signals for the configuration with a minimal amount of fiber in the beam is compared to the signals received when a larger amount of fiber is irradiated. Separate calibration was performed for the 6MV flattened (6x), 6MV flattening-filter free (6FFF), 10x, and 10FFF beam configurations by irradiating the fiber located at Dmax with 200 Monitor Units (MU) in a 6x6cm^2 beam to the 'minimum' and 'maximum' fiber

geometries in a tank of water. The web interface of the MAX SD allows for easy selection of a prior calibration to apply to future measurements.

The W2 also comes with a specially designed slab of Solid Water® (Sun Nuclear Corporation, Melbourne, Florida) material for calibrating large fields (Figure 8). The calibration procedure is similar but with a field size of 30x30cm^2. Output factors were normalized to 4x4cm^2 field size for comparison.

Figure 8. Large Field Calibration slab for the W2.

1.6 Radiation measurements.

All measurements were made using a Varian TrueBeam (Varian Medical Systems UK, Crawley, United Kingdom) linear accelerator (SN:4180) equipped with the Millennium HD120 MLC package. Field shaping was done with the multileaf collimators (MLC), and the jaws were retracted 1cm behind the MLC. The majority of radiation treatments today are shaped using MLC, but the jaws are required to block leakage between the leaves outside of the target area. MLC leaves have rounded edges that are designed to produce

a consistent penumbra across the useful range of motion that would be disturbed if the jaw was aligned to the leaf edge.

Prior to any measurement, the active volume of the W2-1x1 fiber was located at Dmax and centered in the field using the Medphysto software paired with a Beamscan Watertank (PTW, Freiberg, Germany). Output factors were measured by delivering 200MU at 600 MU/min at a 95cm SSD (flattened fields) or 800 MU/min at 100cm SSD (FFF fields) for field sizes ranging from 0.5 to 12 cm. SSD varied between FFF and non-flattened fields to match commissioning data. Fields were MLC shaped and the collimator was rotated 0° to place the MLC motion axis perpendicular to the fiber axis. Measurements were made using the built-in trigger function of the MAX SD, with a rising threshold of 160 pA and a falling threshold of 100 pA. Because the W2 was calibrated for small fields, values were normalized to a 4x4cm^2 field. Repeat measurements were made with the W2 calibrated using the large-field calibration slab to compare the different calibrations under small field measurements.

Dose rate dependencies were measured by irradiating the fiber centered in a 4x4cm^2 field at Dmax with a fixed number of MU. Response was measured for 5 to 600 MU/min for flattened beams, from 400 to 1400 for the 6FFF beam, and from 400 to 2400 for the 10FFF beam. Readings below 10 MU/min had to be manually acquired since the signal was lower than the normal trigger threshold. The signal was normalized to the number of MU delivered.

Dose linearity was measured by delivering 1 to 1000 MU at 600 MU/min (800 for 10FFF) to the fiber centered in a 4x4cm^2 field at Dmax in water. Measurements were

made with trigger start and stop values of 160pA and 100pA. These measurements were repeated 3 times to investigate the consistency of the measurement, the average was normalized to the maximum reading for each energy.

Detector anisotropy was measured using a Standard Imaging LUCY 3D phantom. The phantom is designed to place the active region of the fiber at isocenter (marked by lasers). A 4x4cm^2 field was used to deliver 100 MU with the gantry rotated from 0 to 180° in 5° increments. Zero degrees placed the fiber pointing away from the Linac source. The set-up is shown in Figure 9. Care was taken to minimize the fiber optics irradiated.

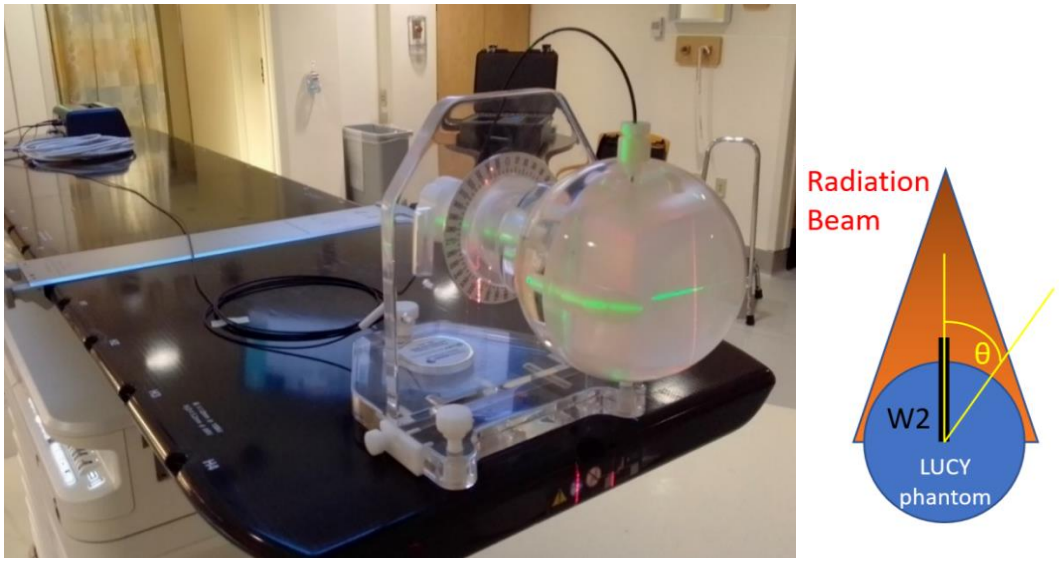

Figure 9. LUCY Phantom set up for W2 Anisotropy measurements. The marks on the phantom coincide with the active scintillation volume and were aligned to room lasers before irradiation under a 4x4cm^2 beam. Simplified model of the set-up is shown on the right.

Beam profiles were measured using the discrete step scanning function of the Beamscan water tank. The signal was collected at depths of 5 and 10 cm over 1 second in

1mm increments moving at 2mm/s. MLC shaped 10x10cm^2 and 4x4cm^2 fields at 6x and 10x energies were delivered at 600MU/min. The proportional current output from the MAX SD provided a signal to the tank's built-in electrometer to pair the location and measurement data. The W2-1x3 detector (SN: XAY191917) was also used to scan 6x 10x10cm^2 and 4x4cm^2 to investigate the effects on signal noise. Measurements were made with the fiber axis perpendicular to the MLC axis. Profiles measured with the W2 were compared to the commissioning data for the Linac measured with a microDiamond detector, and relevant beam metrics were processed in Medphysto Navigator BEAMSCAN software (PTW, Freiburg, Germany, version 4.2.1). W2 profile measurements were not smoothed. All profiles were normalized to their central dose level, field size (FS) was measured at the 50% dose level (full width, half max), penumbra was the distance measured between the 80/20% dose levels, and flatness was measured as (Max-min) / (Max + min) x100% of the beam profile over the central 80% of the field size, per standard definitions of each respective characteristic (Mcdermott, 2018). BEAMSCAN uses linear interpolation when calculating the location of select dose levels.

Results

Figure 10 shows the output factors measured with the W2 for 6MV flattened and FFF beam in comparison to the microDiamond, normalized to the output at 4x4cm^2 field size. Above a 1x1cm^2 field size, both detectors agreed within 2%. The flattened beam saw a 45% higher output for the 0.5x0.5cm^2 field when measured with the W2 in comparison to the microDiamond. Similar behavior was seen at 10MV as shown in Figure 11. The

flattened beam agreed within 2% above 1x1cm^2, but 0.5x0.5cm^2 fields measured 48% higher with the W2. 10MV FFF OF all agreed to within 1%.

Comparison between the output factors between the W2-1x1 and W2-1x3 configuration is shown in Figure 12. Noting that both output factors were normalized to the 4x4cm^2 field, there is a significant difference between the measurements for all field sizes. 3x3cm^2 OF decreased by at least 1% when measured using the large field calibration, 1x1cm^2 fields differed by 5-8%, and at the smallest field differences greater than 12% were measured for the FFF beams and the flattened beams differed by 15% or more.

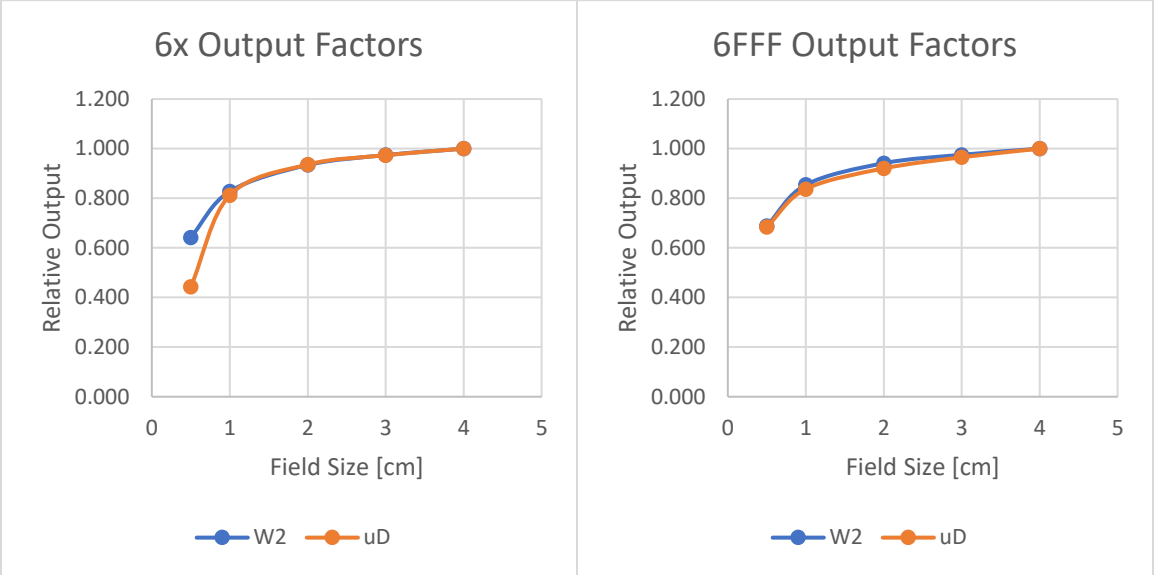

Figure 10. 6MV Small Square Field Output Factors measured with the microDiamond and the W2 at 5cm depth in water. Flattened fields measured with an SSD of 95 cm. Flattening filter free measured at 100cm. Output factors are normalized to a 4x4cm^2 field.

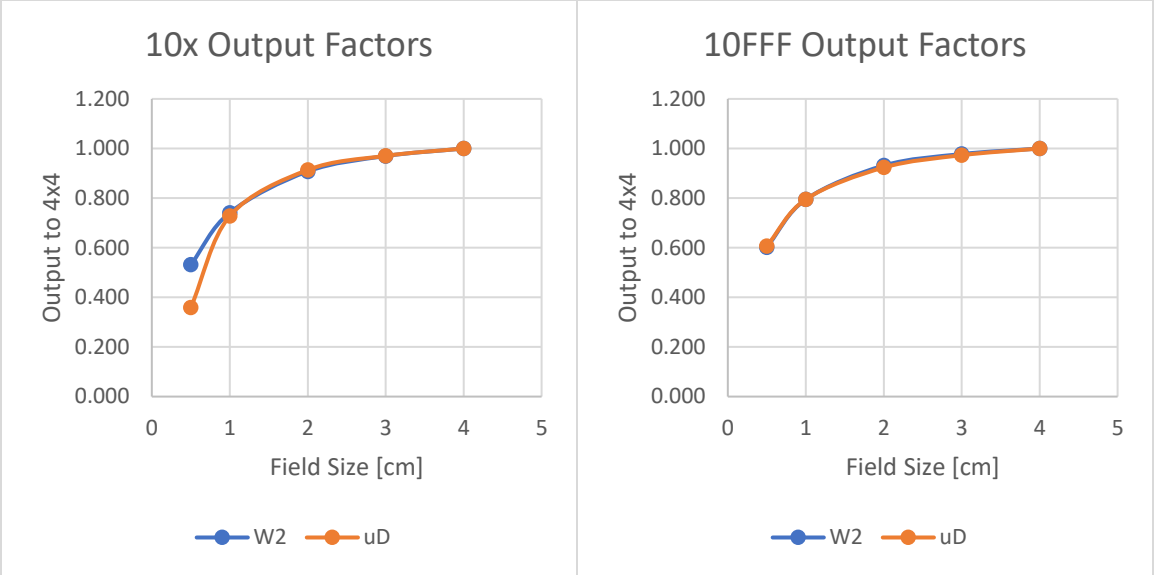

Figure 11. 10MV Small Square Field Output Factors measured with the microDiamond and the W2 at 5cm depth in water. Flattened fields measured with an SSD of 95 cm. Flattening filter free measured at 100cm. Output factors are normalized to a 4x4cm^2 field.

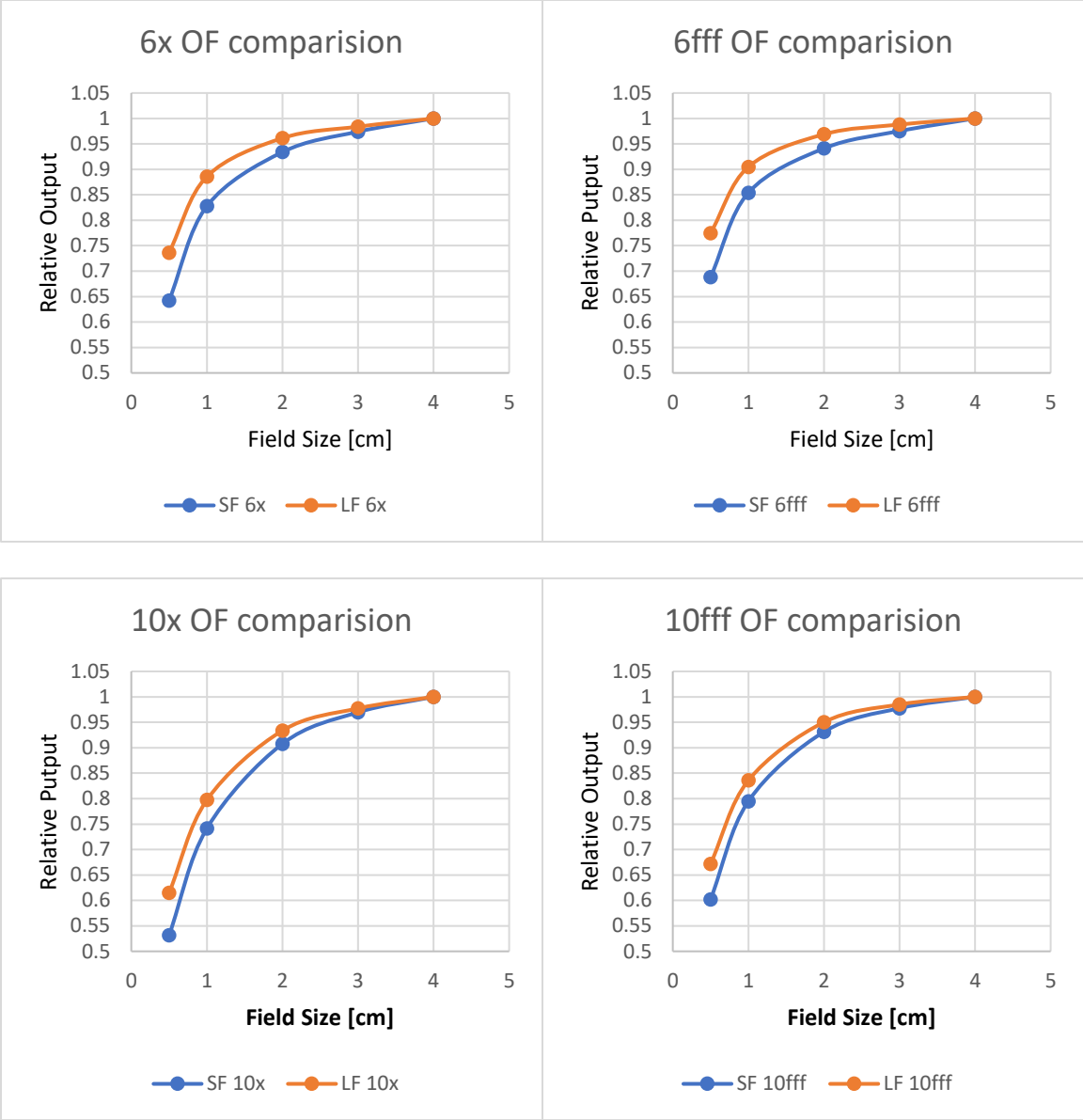

Figure 12. Small Field and Large Field Calibration Difference. Comparison of the output factor at small fields when calibrated with the small field holder (6x6cm^2) and the large field holder (30x30cm^2). Output factors are normalized to a 4x4cm^2 field.

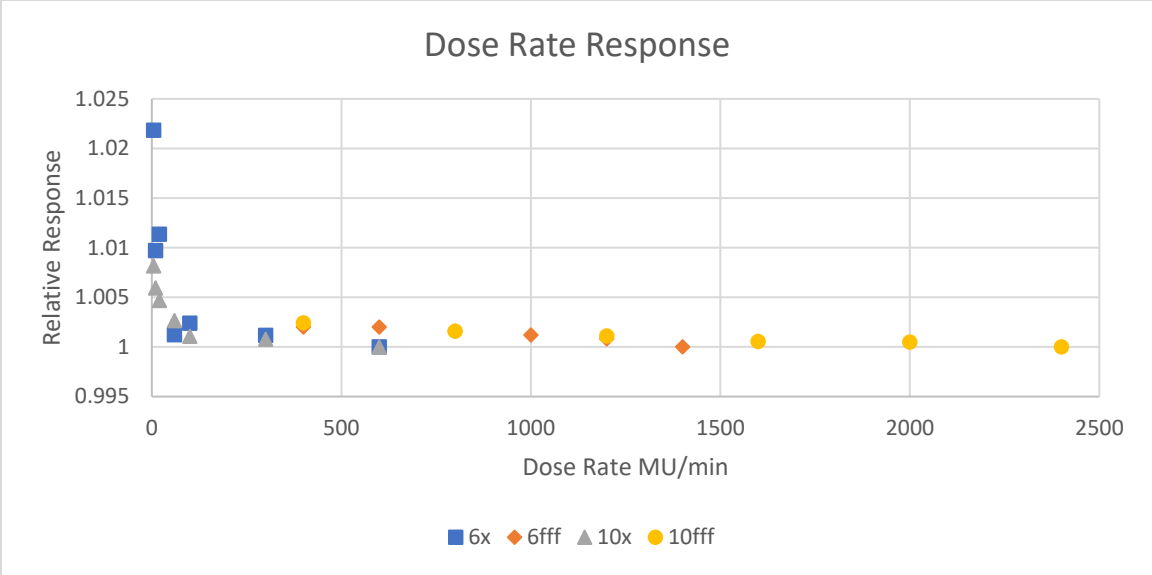

Figure 13. Dose Rate Response of the W2 in water at Dmax for a 5x5cm^2 field with an SSD of 100cm. Normalized to the highest dose rate. Below 5MU/minute, measurement was manually started and stopped as the signal was below the trigger threshold.

Dose rate linearity, shown in Figure 13, was linear within 0.25% for all FFF beams. 10MV beams delivered at 60 cGy/min were linear within 0.25% and were under 0.5% above 20cGy/min, but the response increased to 1% with lower rates. 6MV was only linear within 0.5% above 60cGy/min, with measurements below 20cGy/minute aligning within 2.2%. The inconsistencies at the lowest dose rates are likely due to the uncertainties stemming from manual control of starting and stopping the measurement since the trigger was unreliable at dose rates below 20MU/Min.

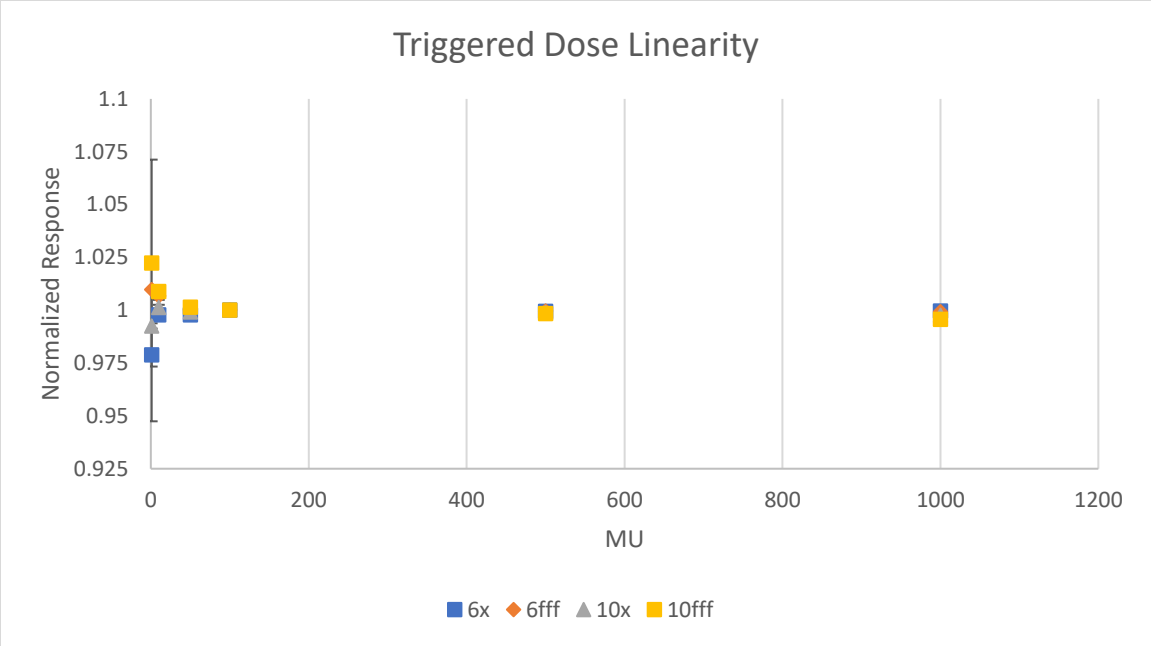

Figure 14. Dose Rate Linearity of the W2 in water at Dmax for a 5x5cm^2 field with an SSD of 100cm. Normalized to the response at 100MU. Error bars are ± 1 SD.

Shown in Figure 14, absolute dose measurements were all within 2.2%, with measurements above 10cGy linear within 1%. Standard deviations of measurements above 10cGy were below 0.25%, with standard deviations of up to 5% at 1 cGy. This increase in uncertainty is likely due to baseline noise becoming significant at low doses.

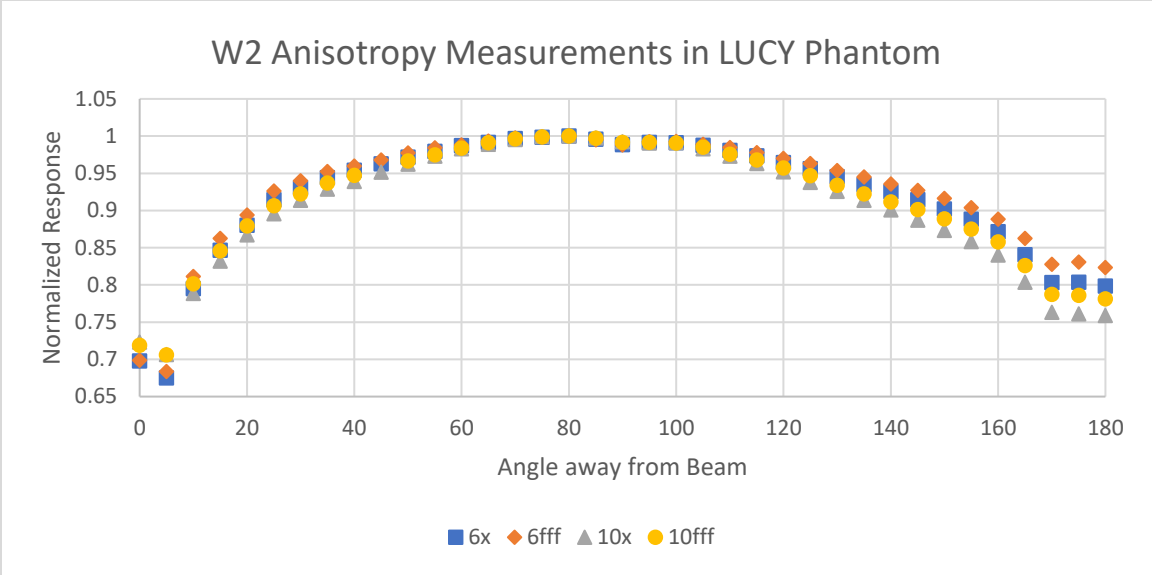

Figure 15. Anisotropic response of the W2 in a Standard Imaging LUCY phantom. 0° references the beam along the fiber axis; 180° points the W2 directly into the beam. 100MU were delivered through a 4x4cm² field at the max dose rate.

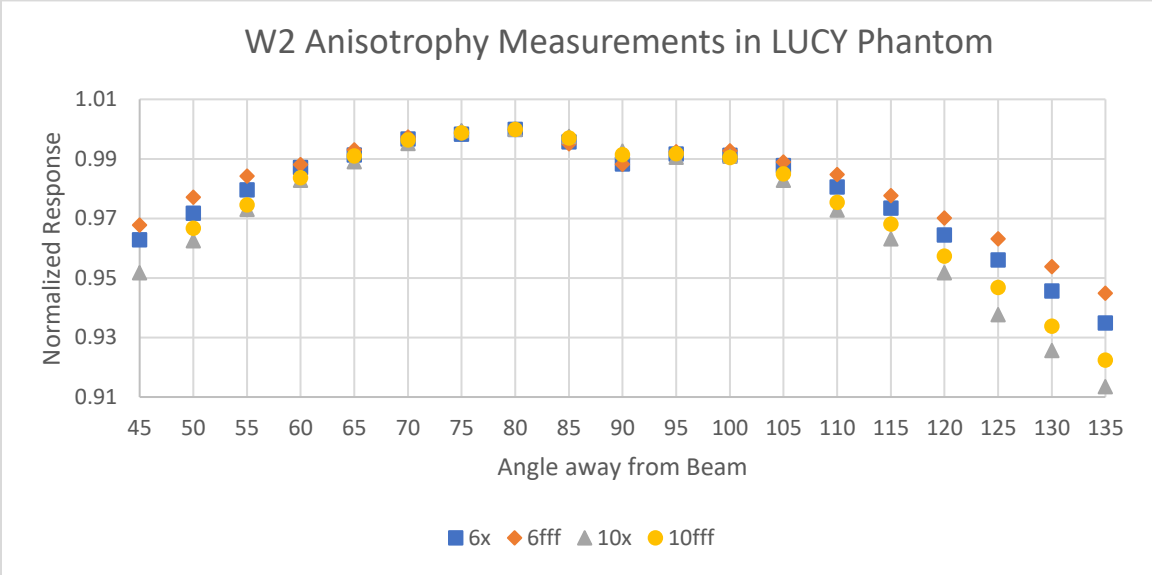

Figure 16. Anisotropic response of the W2 in a Standard Imaging LUCY phantom, focusing on the 90° ± 45° range to show detail. 100MU were delivered through a 4x4cm² field at the max dose rate.

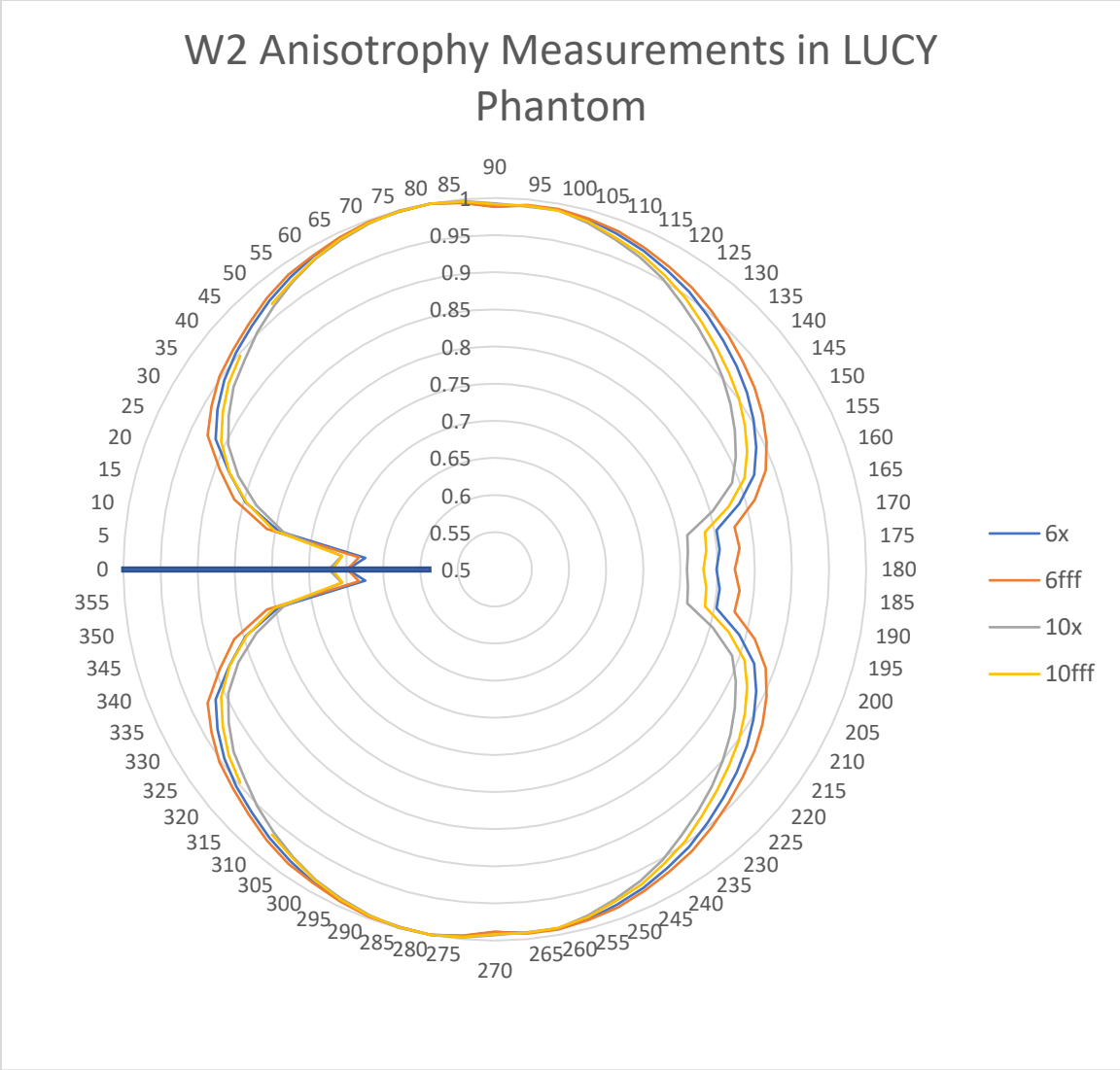

Figure 17. Polar representation of the W2 anisotropy data measured in a LUCY phantom. The bar indicates the orientation of the W2 with the fiber continuing off to the left. 100MU was delivered through a 4x4cm^2 field at the maximum allowed dose rate. Note the range has been decreased to show detail and the data was symmetrized from 0°-180°.

Anisotropy measured with the LUCY phantom is shown across all angles in Figure 15 and a narrower range centered around the perpendicular 90° in Figure 16. All energies saw the maximum response at 80°. Deviations were under 1% from 70° to 100° but

response would quickly fall off moving away from perpendicular. 6FFF showed the least dependency and 10x showed the greatest angular dependency, with a response as low as 0.706 at 0°. Figure 17 represents the same information in polar form. The data was symmetrized.

6MV, 4x4	W2-1x1	W2-1x3	uD		6MV, 10x10	W2-1x1	W2-1x3	uD
FS	4.114	4.125	3.974		**FS**	10.377	10.401	10.455
Penumbra Lt	3.22	3.2	2.93		**Penumbra Lt**	3.62	3.61	3.66
Penumbra Rt	3.21	3.25	2.97		**Penumbra Rt**	3.48	3.56	3.74
Flatness%	106.33	106.05	103.53		**Flatness%**	102.49	102.42	103.55

Table 2. Beam Profile Characteristics for 6MV flattened beam profiles at 5cm depth in water. Field size and penumbra widths reported in mm. Comparison between W2 1x1, W2 1x3, and microDiamond.

10MV, 4x4	W2-1x1	uD		10MV, 10x10	W2-1x1	uD
FS	4.112	4.118		**FS**	10.38	10.458
Penumbra Lt	3.17	4.04		**Penumbra Lt**	4.65	4.44
Penumbra Rt	3.21	4.02		**Penumbra Rt**	4.41	4.47
Flatness	106.01	108.9		**Flatness**	102.89	103.27

Table 3. Beam Profile Characteristics for 10MV flattened beam profiles at 5cm depth in water. Field size and penumbra widths reported in mm. Comparison between W2 1x1 and microDiamond.

Specific size characteristics of the beam profiles shown in Figure 18 through Figure 22 are summarized in Table 2 (6MV beams) and Table 3 (10MV beams). Between the 1x1 and 1x3 versions of the W2, measurements agreed within 0.1 mm when scanning laterally. The microDiamond measured the 6MV 4x4cm^2 field as 0.15mm narrower than the average

of the W2 measurements, and the penumbra measurements were between 0.29 and 0.27 mm narrower. The profile measured flatter with the microDiamond. At 10MV, the microDiamond measured the penumbra as more than 0.8mm wider than the W2 and showed a less flat profile. At 10x10cm^2 field sizes, the critical dimensions were within 0.2mm and flatness was consistent between the devices.

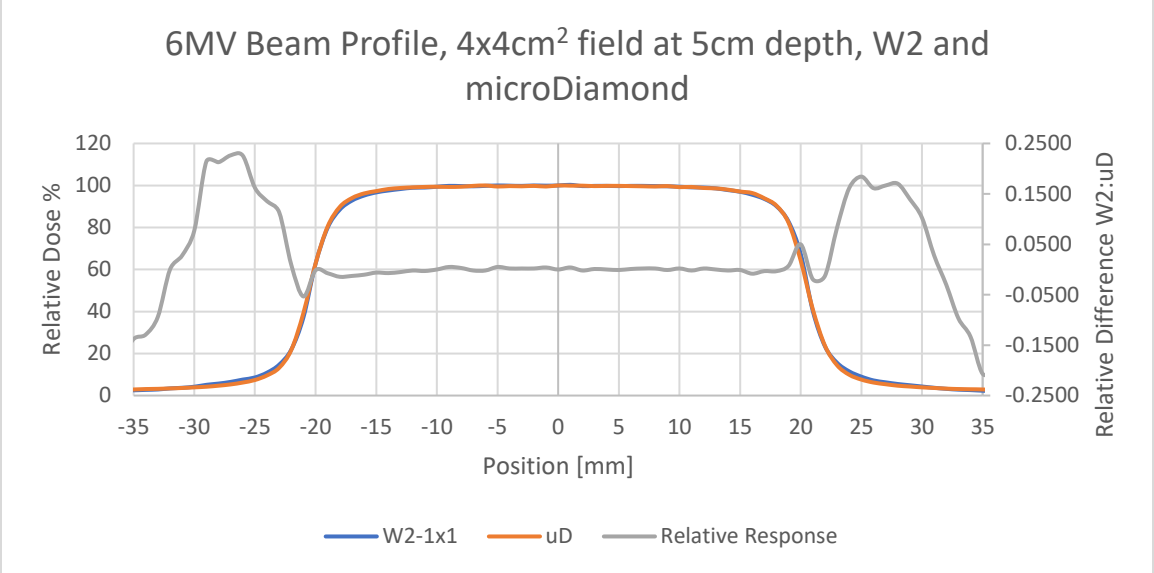

Figure 18. 6MV beam dose profile comparing the Exradin W2 to the PTW microDiamond for a 4x4cm^2 field size at a depth of 5cm in water.

Within the central region and the penumbra of the 6MV 4x4cm^2 beam (Figure 18), measurements closely aligned within 1.5%. In the centimeter outside of the penumbra, the W2 measured significantly higher than the microDiamond, but this quickly inverted with the microDiamond reading a higher dose in the far lateral regions. In all other profiles, the microDiamond showed a higher response below the 5% dose level compared to the W2. The 10MV small field profile in Figure 21 showed the greatest difference in profile shape between the detectors. The microDiamond exhibited more rounding of the outer portions of the main beam and showed a more gradual falloff outside the penumbra

(evident by the curvature of the relative difference and the strong inflection passing through the penumbra).

The profiles were symmetric when scanned laterally, indicating that the Cherenkov contamination was correctly accounted for during the measurements. For illustrative purposes, Figure 23 shows how the Cherenkov contamination can have a significant effect on the measurement. This profile was scanned moving the detector through the field parallel to the fiber's axis and shows a steady increase in reading as the amount of fiber in the beam increases.

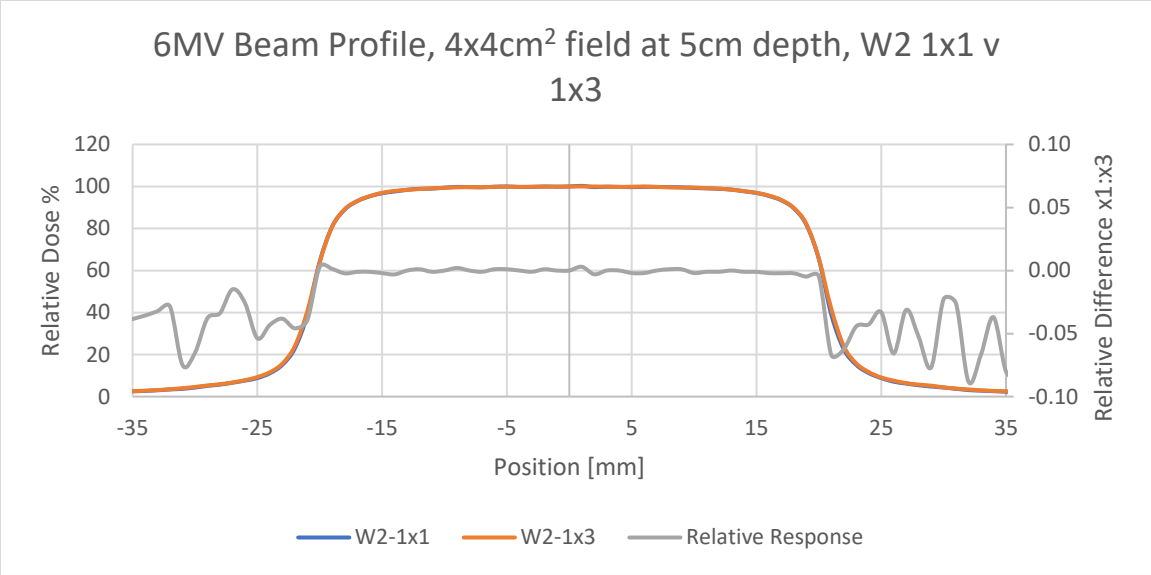

Figure 19. 6MV beam dose profile comparing the Exradin W2 1x1 and 1x3 detectors for a 4x4cm² field size at a depth of 5cm in water.

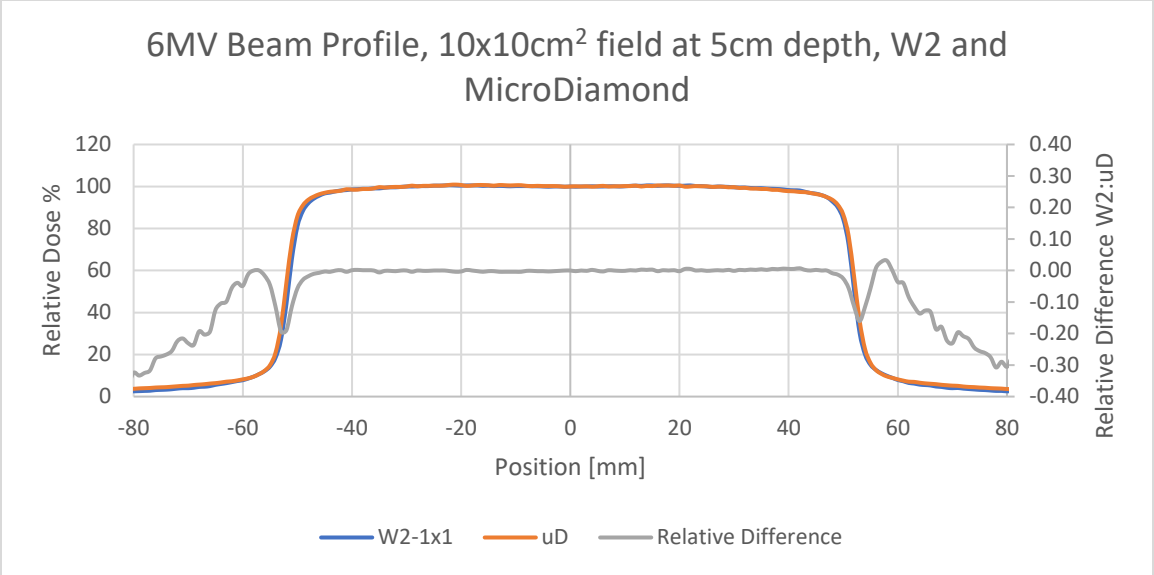

Figure 20. 6MV beam dose profile comparing the Exradin W2 to the PTW microDiamond for a 10x10cm^2 field size at a depth of 5cm.

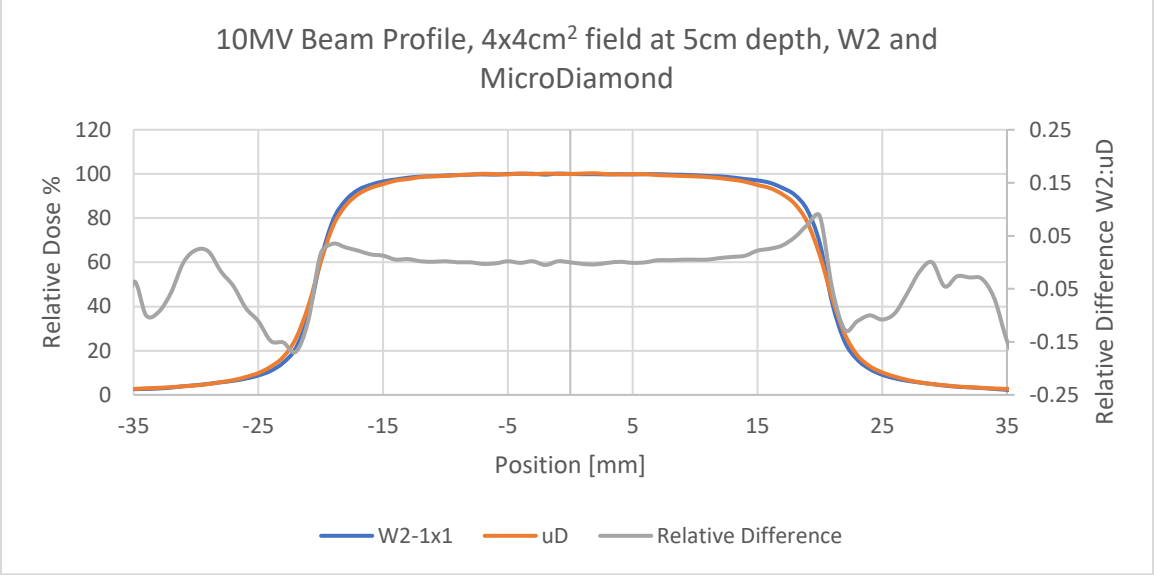

Figure 21. 10MV beam dose profile comparing the Exradin W2 to the PTW microDiamond for a 4x4cm^2 field size at a depth of 5cm.

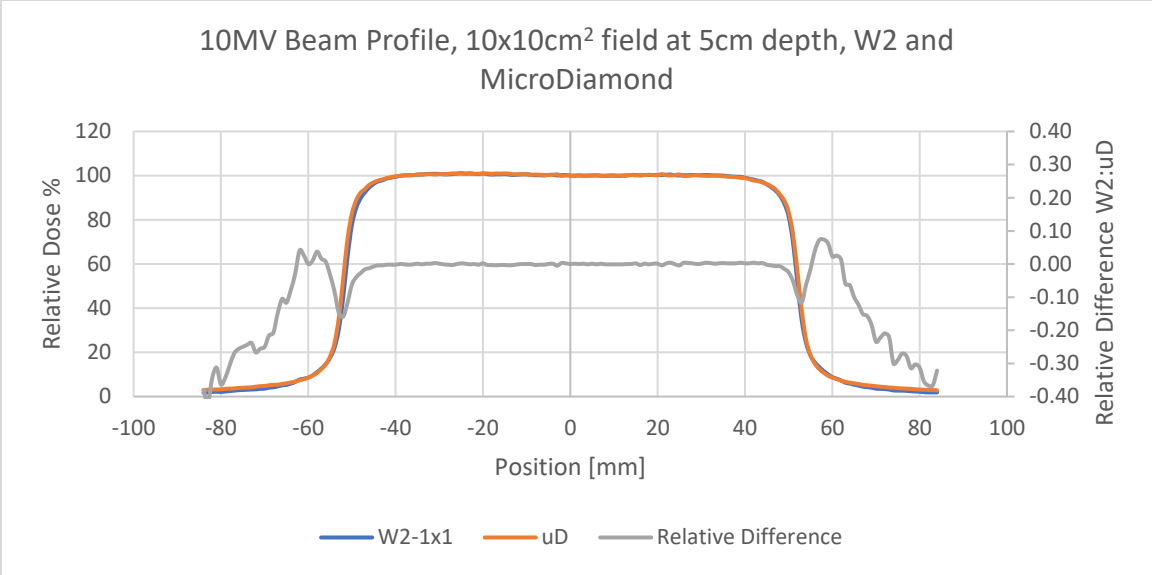

Figure 22. 6MV beam dose profile comparing the Exradin W2 to the PTW microDiamond for a 10x10cm² field size at a depth of 5cm.

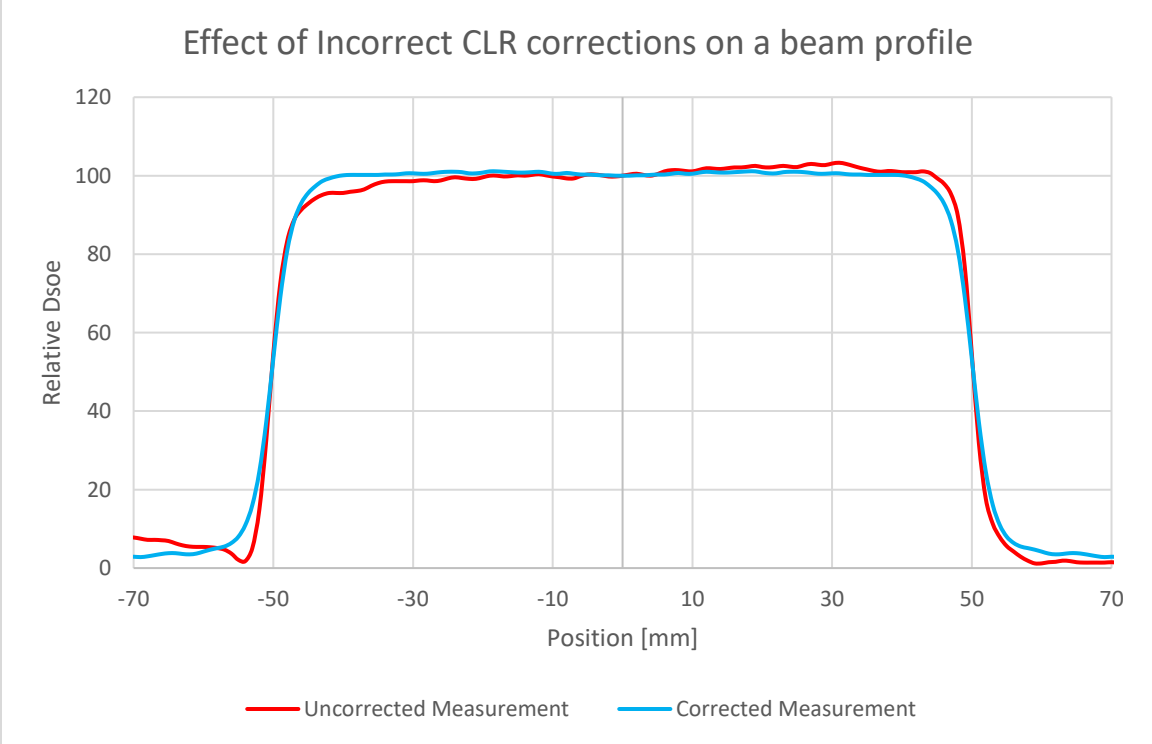

Figure 23. Example of an incorrectly calibrated profile measurement. 6MV 10x10cm² jaw field measured at Dmax in water.

Discussion

The increase in measured output factor at the 0.5x0.5cm^2 field size in comparison to the microDiamond has the potential to be clinically significant, as the dose calculation algorithms for highly modulated EBRT beams require accurate characterization of small beamlets. The 2.2mm diameter active volume (compared to the 1mm diameter W2) may be suffering from partial volume averaging and non-uniform occlusion of the source, reducing the measured output. If this were due to a change in the energy spectrum at small fields, such as an increase in scatter components in the spectrum (Junell, 2013), it would be expected that the microDiamond would measure a higher output due to the increased low-energy response of diodes and diamond detectors.

As shown in Tables 1 and 2 and the beam profiles, the differences between how the W2 and the microDiamond measured beam feature sizes were small. This could indicate that at this scale, the partial volume effect is similar between the two. However, when comparing the profiles of the 4x4cm^2 fields, shown in Figure 18 and Figure 21, there is evidence that the microDiamond is exhibiting stronger partial volume averaging. Focusing on the shoulders of the profile (transitions of in-field to penumbra and penumbra to out-of-field), there is a slight inflection that indicated that the W2 is reading higher approaching the field edge, and then flattens out in the low dose sooner than the microDiamond. The broader shoulders of the microDiamond could be due to the detector averaging parts of the penumbra region into the low or high dose areas.

Outside of the penumbra region where scatter radiation is the dominant contributor to absorbed dose, energy dependence can significantly affect the readings between different detectors. Out-of-field dose estimates are often required in RT treatments when

a patient had electronic implants or is pregnant, and treatment planning systems are often inaccurate at any significant distance from field edges. In the far regions measured, the W2 always reported a lower dose than the microDiamond. The increased low energy response of the microDiamond compared to the W2 is due to the increased Z equivalence of the material. Since the W2 is water equivalent and it shows a more consistent response, it could be a useful tool for out-of-field dosimetry if it were not for the low SNR due to the reduced signal from such a small active volume. Time or machine output could be scaled to reduce the relative noise if such a measurement was made with this detector.

Dose responses were very consistent across most clinically relevant dose magnitudes and rate. The uncertainty at doses of 1cGy and 10cGy are likely dominated by noise and delays with the trigger mechanism and only a handful of pulses will be produced. Dose rates below 60cGy/minute saw the largest uncertainties and standard deviations, but that is also likely caused by noise. The actual impact of these variations is exceptionally small, however, (excluding 6x at 1cGy/minute) as any measurement above 10cGy in magnitude or 20cGy/minute were all within 1% of the expected response, with even more accurate readings at higher amounts. This wide dynamic range is important for measurements of modulated fields, as the dose rate to a point will rapidly fluctuate as the machine output and field shaping modulate the beam.

The anisotropy of the W2 outside of its radial axis is the most significant downfall. When measuring static fields such as small field outputs or profiles, there will not be any angular dependencies and calibration for a given orientation would be straightforward. However, if the detector were to be used for quality assurance (QA) point measurements,

whether patient specific, end-to-end, or machine verification, care must be taken to ensure that the fiber axis is in line with the gantry rotational axis. Prior characterization of the similar W1 detector found the radial dependencies to be within 0.21% (Carrasco, 2016). For some head and neck, abdominal, or pelvic cases this would be easy to ensure.

Cranial cases, especially stereotactic cases where the smallest field sizes are often seen, typically allow for numerous table positions that can be taken advantage of to improve conformality of dose to the target or to increase tissue sparing and avoidance. If the W2 were placed parallel to the treatment couch and that couch were rotated, the gantry would no longer be rotating around the radial dimension of the detector and the response would vary significantly depending on the gantry position. The impact on measurements made at different couch angles could be quantified using the SNC StereoPHAN (Sun Nuclear Corporation, Melbourne, Florida) to simulate cranial treatment geometries. It could be possible to develop software to pair the current measurement data with information from the Linac about its current gantry angle, but that could be sensitive to small uncertainties in angle and machine information may not be readily accessible. Avoiding the angular dependency could be accomplished by removing the couch rotations during QA, but that defeats the purpose of trying to get the most precise point measurement possible because couch walk-out of up to 1mm can be present in stereotactic treatments (AAPM TG 142, 2009). These changes would be significant in relation to the size of the detector. Any significant gradient would only exacerbate the challenges to an accurate measurement.

The peak response at 80° is an interesting finding, but there are potential mechanisms for this behavior. One explanation could be that this is the optimal angle for visible photon

emission from the scintillating material with minimal self-attenuating of the low energy photons. While CPE is required in the local region to obtain an accurate measure of dose, small perturbations of the CPE at the scintillator material boundary could result in inhomogeneous scintillation across the active volume. If the response were influenced significantly by Cherenkov contamination, it would be expected that a peak response would have been seen near 140° or 40° as Cherenkov photons travel outwards at approximately 40° from the direction of the particle motion and that would place the photons in line with the fiber optics resulting in the shortest path with the fewest chances for attenuation or absorption (Rongxiao, 2013).

Qualitatively, the W2 is more challenging and time consuming to use compared to most other diode or air ionization chambers. Calibration for the Cherenkov correction can be sensitive to set-up, and any error in calibration can result in a significantly erroneous reading. Figure 23 shows how a beam profile can be significantly distorted as more fiber is irradiated. In a static field, this could result in severely over or under-reporting an output factor or point measurement with little indication that it is incorrect. When calibrated, the effects of fiber irradiation are minimized but are not eliminated. Figure 12 shows how the output factors for small fields vary when different calibration set-ups are used and that the output factor can significantly differ at 2cm and below. It is important to select the right calibration for the expected range of radiation sizes to be measured.

This study has several strengths, but the key strength is that this is a fully independent characterization of the W2. Not only is it important to externally verify a manufacture's claims, but other clinics should have multiple references available to compare to when commissioning their own detectors. It also has produced some interesting findings that can

be followed up in future studies, namely some significant difference in very small field output factors.

There are some limitations that should be addressed in any future study. First, there is little statistical analysis of the performance and there is no characterization of the noise properties. At low dose rates specifically, the standard error of the measurements far exceeded the actual differences in measurements, and in out-of-field locations noise may dominate the measurement. Further characterization of the anisotropy could be investigated using a StereoPHAN at more couch angles, and information about the radial response could be included. More detectors included in comparison, in addition to possible Monte Carlo simulation, would aid in determining which measurement method produces the most accurate results and, in conjunction with TRS-483 (IAEA, 2017), could help verify the accuracy of any correction factors needed.

Summary and Conclusions

In this study, we independently characterized the anisotropy, dose linearity, and dose rate linearity of the W2 and compared output factor and beam profile measurements against another suitable detector for small field dosimetry. While the spectral analysis internally managed through the MAX SD system can produce stable, consistent measurements for varying fiber irradiations, it is incredibly important to use the appropriate calibrations size (large or small field) to ensure accuracy. The CLR adjustments were not able to completely decouple the measurement from the amount of fiber irradiation, so it is important to limit how much the amount of irradiated fiber changes through a measurement. Beam profiles should be scanned laterally opposed to along the fiber axis through the beam. As the W2-1x1 and W2-1x3 performed almost identically when scanning beam profiles laterally, the W2-1x3 configuration is recommended due to the increased signal from the larger active volume. The W2 appears to slow less partial volume averaging than the microDiamond in the penumbra regions and exhibits a different response to the lower energy scatter spectrum. Significant anisotropy along the detector axis indicates that this detector is not well suitable for QA procedures or point measurements that require a table rotation.

References

AAPM TG 142. (2009). *Task Group 142 report: Quality assurance of medical accelerators.* American Association of Physicists in Medicine.

Alaeian, H. (2014). An Introduction to Cherenkov Radiation. *Stanford University Press*.

Almond, P. R. (1999). AAPM's TG-51 protocol for clinical reference dosimetry of high-energy photon and electron beams. *Medical Physics 26(9)*, 1847-1870.

Borca, V. (2013). Dosimetric characterization of use of GAFCHROMIC EBT3 film for IMRT dose verification. . *Journal of Applied Clinical Medical Physics, V14(2)*.

Bushberg, J. (2011). *The Essential Physics of Medical Imaging.* Lippincott Williams & Wilkins.

Carrasco, P. (2016). Characterization of the Exradin W1 scintillator for use in radiotherapy. . *Medical Physics*.

Das, I. (2008). Small Fields: Nonequilibrium Radiation Dosimetry. *Med Phys 35(1)*, 206-215.

Fernandez, P. (2017). Neutrino Physics in Present and Future Kamioka Water-Cherenkov Detectors with Neutron Tagging. *PhD Dissertation, University Autonomous of Madrid*, 65.

Galavis, P. (2019). Characterization of the Plastic Scintillation Detector Exradin W2 for Small Field Dosimetry. *Med. Phys. 46(5)*.

Guillot, M. (2011). Spectral method for the correction of the Cerenkov light effect in plastic scintillation detector: A comparision study of calibration procedures and validation in Cerenkov kight-dominated situations. *Med. Phys. 38(4)*, 2140-2150.

IAEA. (2017). *Dosimetry of Small Static Fields Used in External Beam Radiotherapy, Technical Reports Series No. 483.* Vienna: IAEA.

Jang, K. W. (2013). Application of Cerenkov radiation generated in plastic optical fibers for therapeutic photon beam dosimetry. *Journal of Biomedical Optics, 18(2)*.

Junell, S. (2013). Dosimetry for small and Nonstandard Field, PhD Dissertation. *University of Wisconsin-Madison*.

Khan, A. U. (2020). Characterizing a PTW microDiamond detector in kilovoltage radiation beams. *Medical Physics 47(9)*, 4553-4562.

Knoll, H. (2010). *Radiation Detection and Measurement.* Danvers, MA: John Wiley & Sons.

Kumar, S. (2012). A patient-specific quality assurance study on absolute dose verification using ionization chambers of different volumes in RapidArc treatments. *Med Dosim*.

L'Annuziata, M. (2016). *Radioactivity: Introduction and History, from the Quantum to Quarks.* Amsterdam, Netherlands: Elsevier Science.

Li, X. (1995). Lateral electron equilibrium and electron contamination in measurements of head-scatter factors using miniphantoms and brass caps. *Med Phys 22*, 1167-1170.

Mcdermott, P. N. (2018). *The Physics and Technology of Radiation Therapy.* Wisconsin: Medical Physics Publishing.

McEwen, M. (2014). Addendum to the AAPM's TG-51 protocol for clinical reference dosimetry of high-energy photon beams. *Medical Physics 41(4)*.

Palmans, H. (2018). Dosimetry of small static fields used in external photon beam radiotherapy: Summary of TRS-483, the IAEA-AAPM international Code of

Practice for reference and relative dose determination. *Medial Physics 45 (11)*, e1123:e1145.

Pierluigi, C. (2019). Real-time Dosimetry with Radiochromic Film. *Scientific Reportq*, 5307.

PTW Frieburg Germany. (2021, June 17). *microDiamond Synthetic Diamond Detectors product page*. Retrieved from PTW The Dosimetry Company: https://www.ptwdosimetry.com/en/products/microdiamond/

Rongxiao, Z. (2013). Superficial Dosimetry Imaging based on Cherenkov Emission for external beam radiotherapy with megavoltage x-ray beam. *Med. Pjhys. 40(10)*.

Standard Imaging. (2018). *MAX SD User Manual, REF 90030.* Middleton, WI: Standard Imaging.

Standard Imaging. (2021, June 17). *Exradin W2 Scintillator product information page*. Retrieved from https://www.standardimaging.com/exradin-detectors/scintillators

Wuerfel, J. (2013). Dose Measurements in Small Fields. *Medical Physics International (1)*, 81-87.

Appendix: Selected Full Size Figures

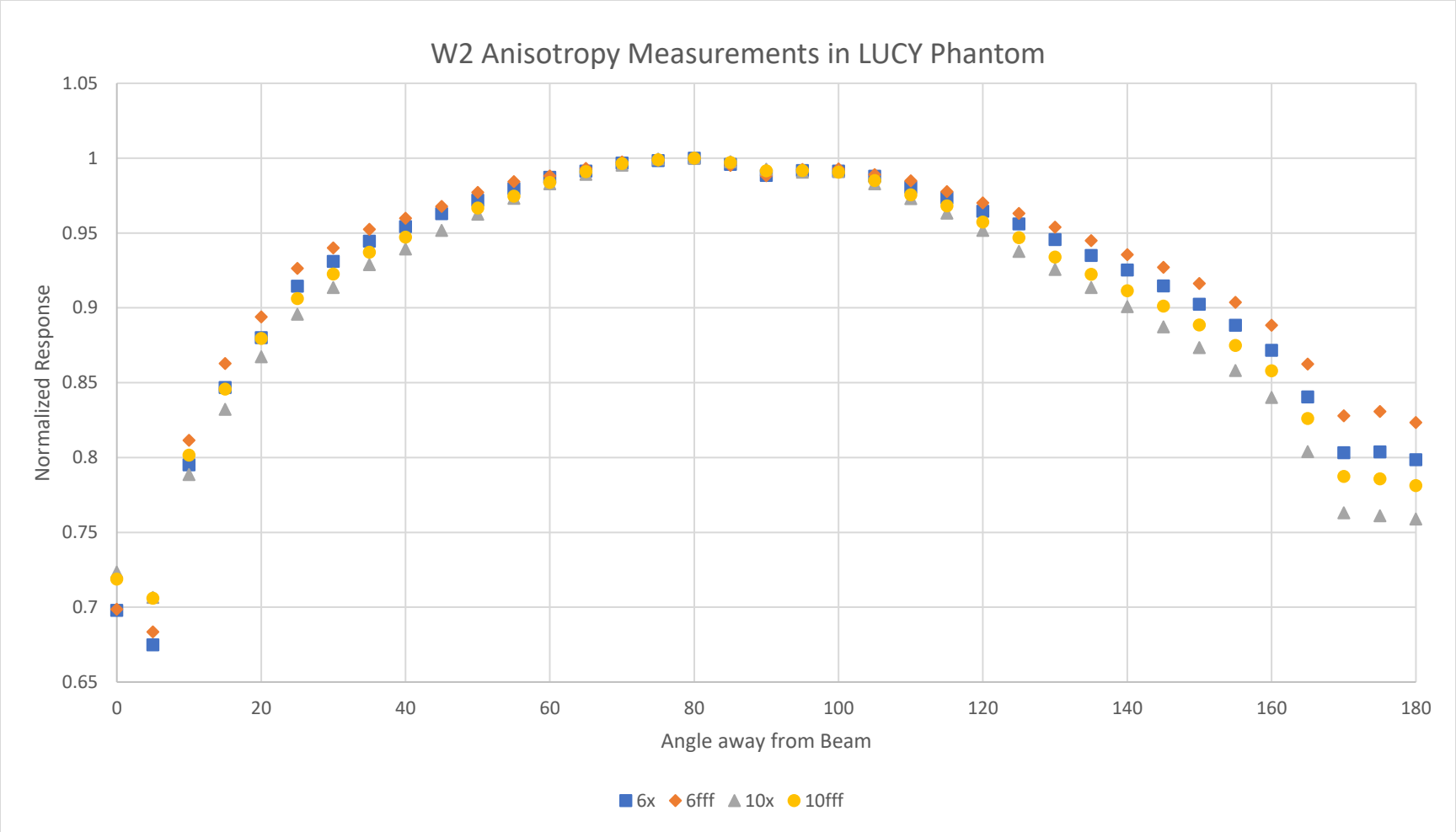

Figure 15. Anisotropic response of the W2 in a Standard Imaging LUCY phantom. 0° references the beam along the fiber axis; 180° points the W2 directly into the beam. 100MU were delivered through a 4x4cm2 field at the max dose rate.

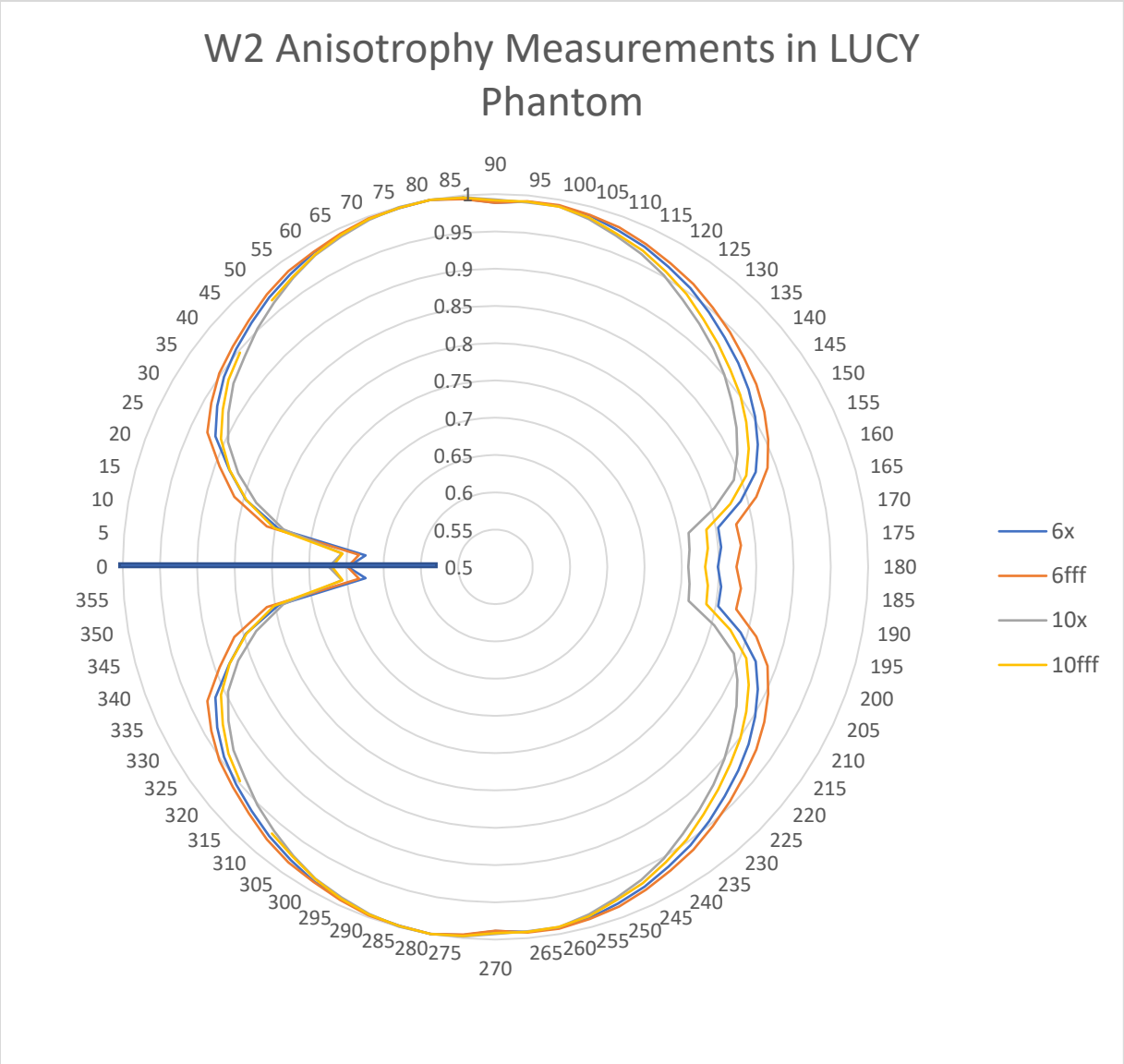

Figure 17. Polar representation of the W2 anisotropy data measured in a LUCY phantom. The bar indicates the orientation of the W2 with the fiber continuing off to the left. 100MU was delivered through a 4x4cm2 field at the maximum allowed dose rate. Note the range has been decreased to show detail and the data was symmetrized from 0°-180°.

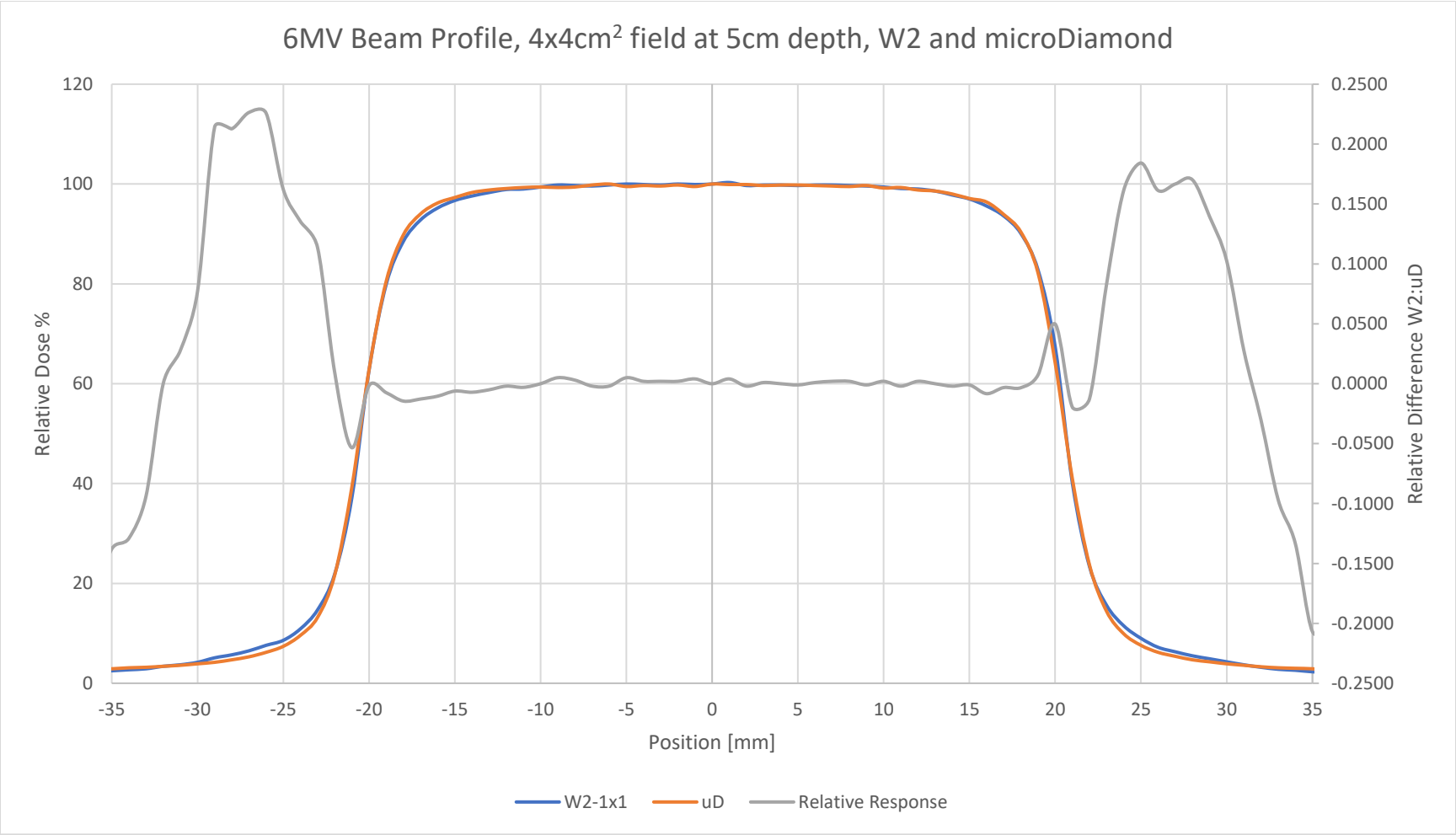

Figure 18. 6MV beam dose profile comparing the Exradin W2 to the PTW microDiamond for a 4x4cm2 field size at a depth of 5cm in water.

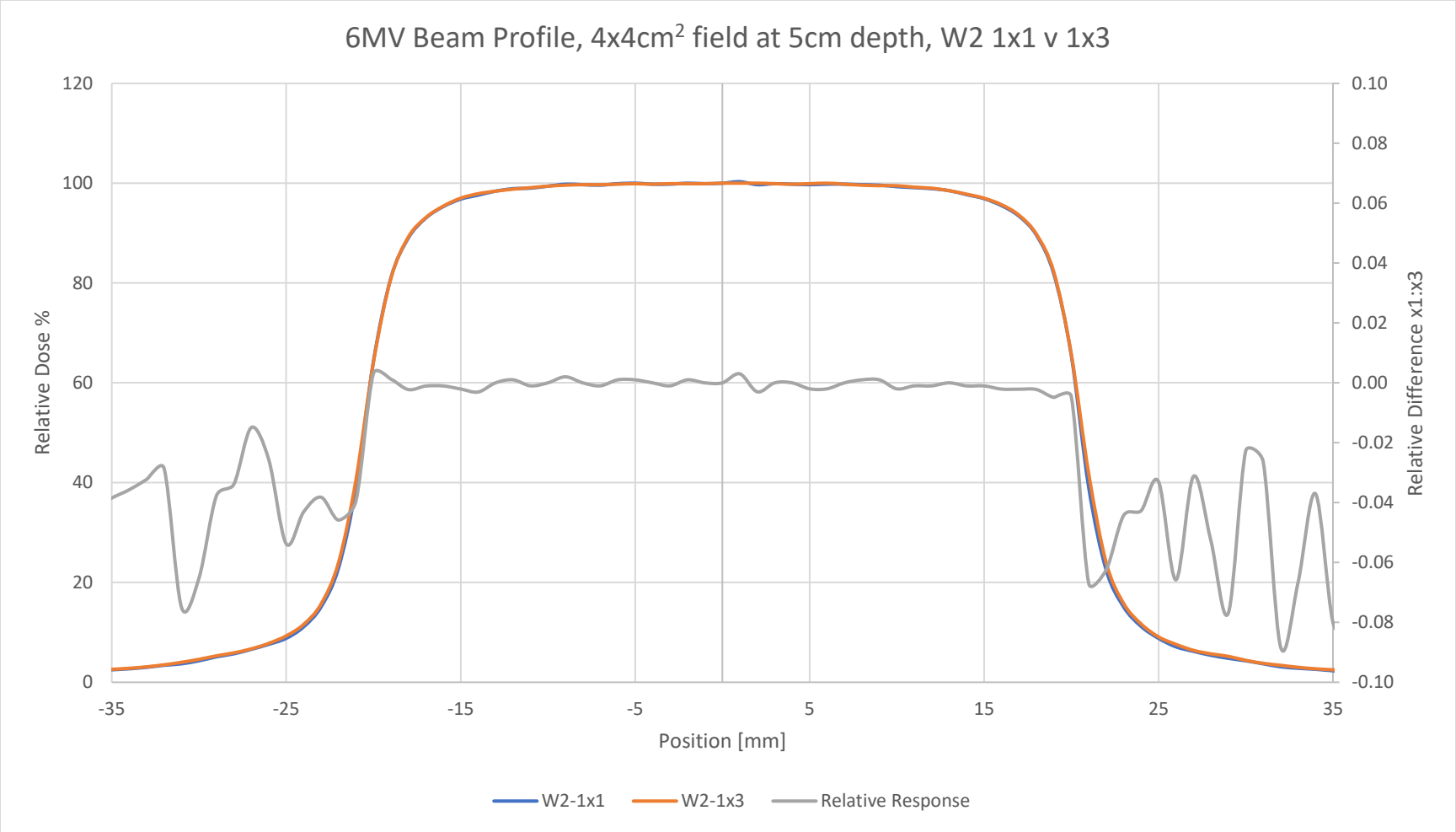

Figure 19. 6MV beam dose profile comparing the Exradin W2 1x1 and 1x3 detectors for a 4x4cm2 field size at a depth of 5cm in water.

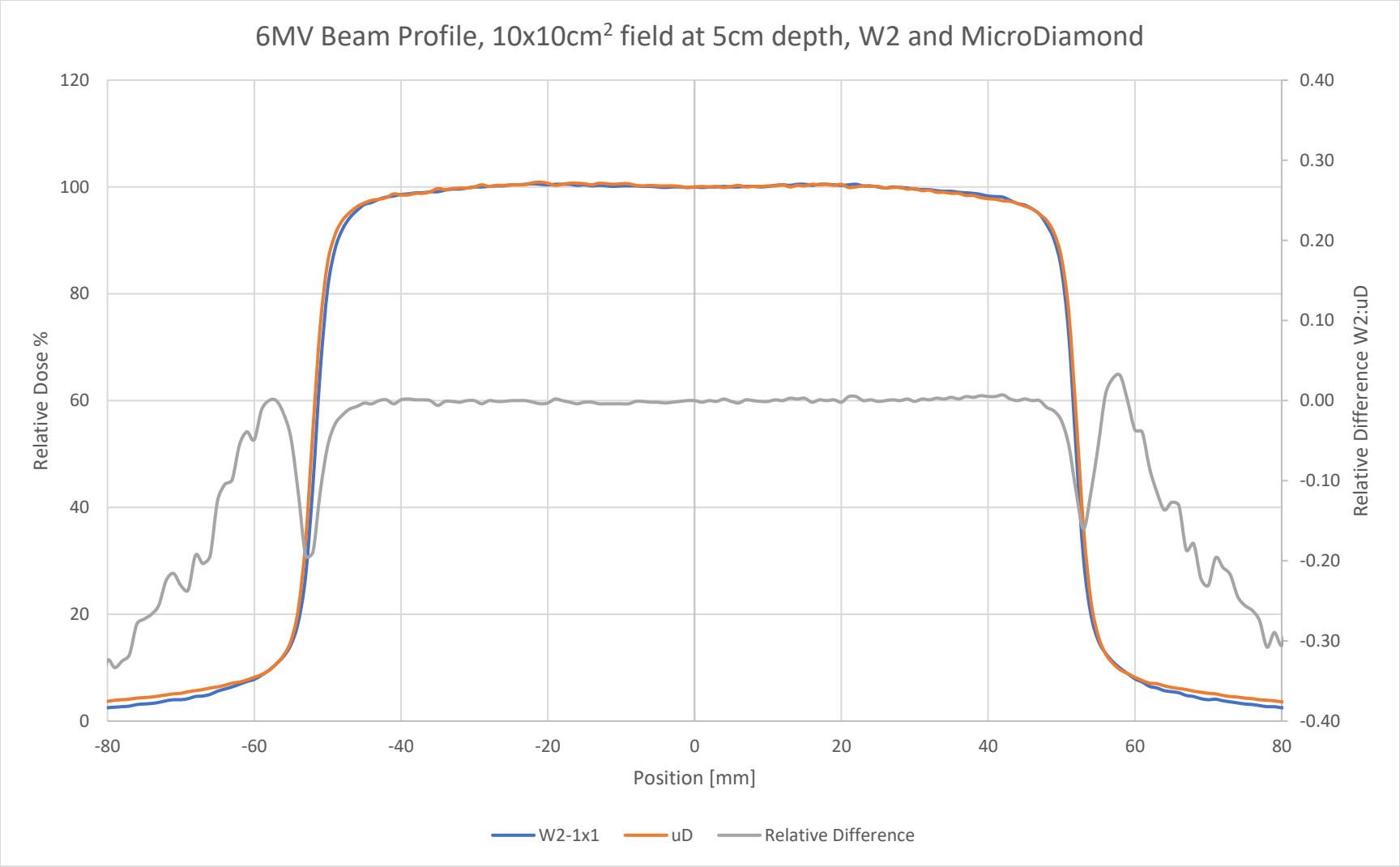

Figure 20. 6MV beam dose profile comparing the Exradin W2 to the PTW microDiamond for a 10x10cm2 field size at a depth of 5cm.

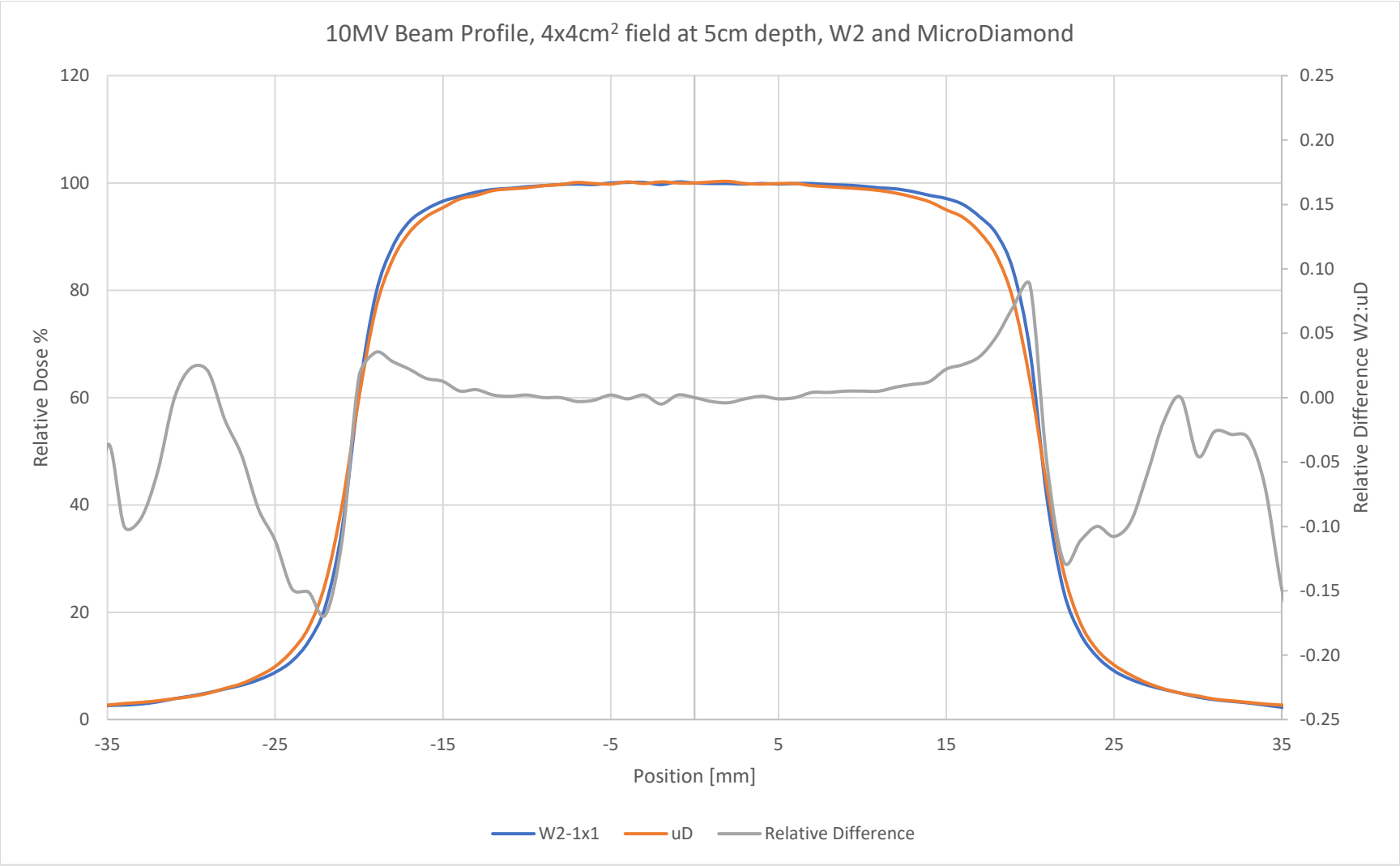

Figure 21. 10MV beam dose profile comparing the Exradin W2 to the PTW microDiamond for a 4x4cm2 field size at a depth of 5cm.

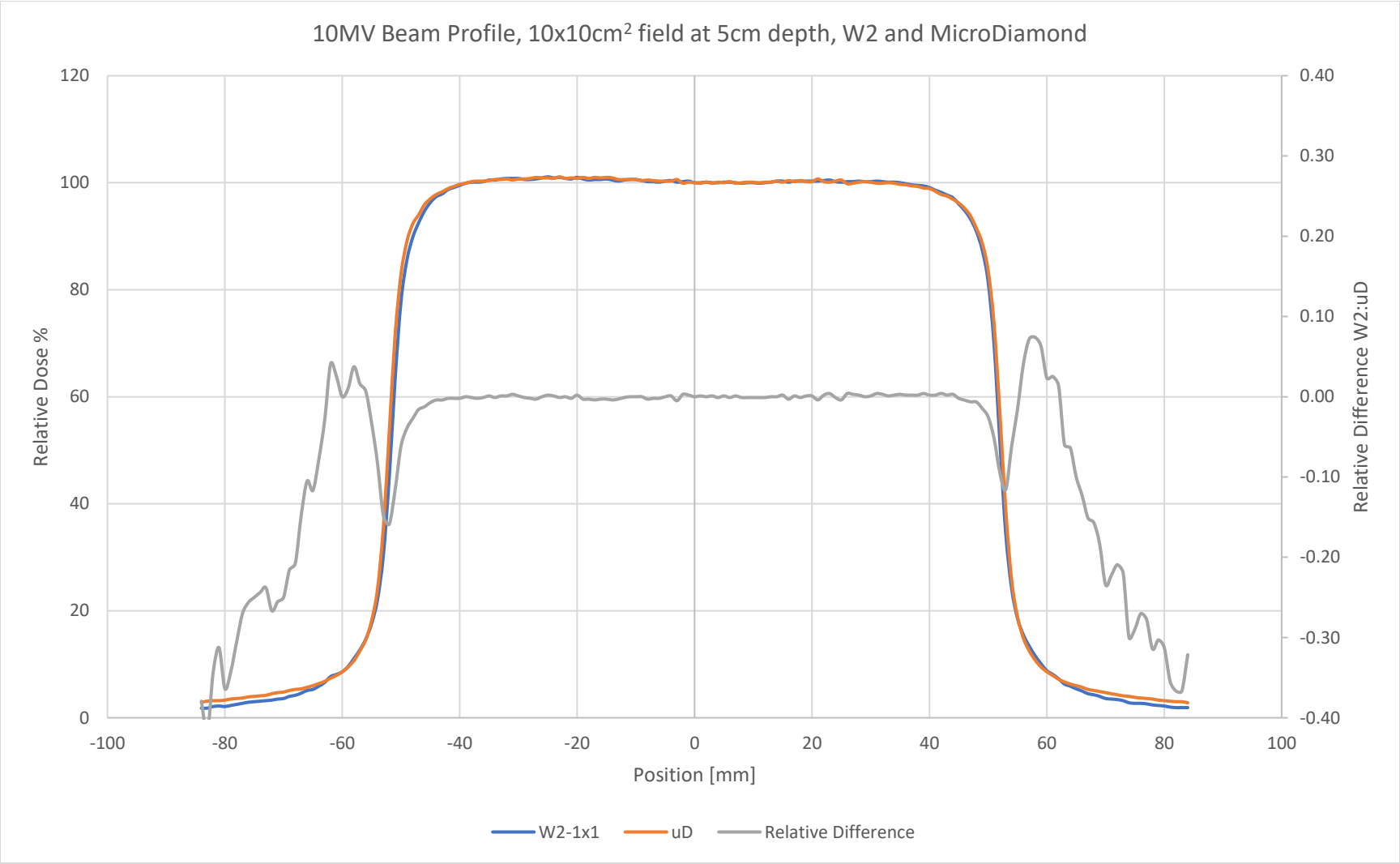

Figure 22. 6MV beam dose profile comparing the Exradin W2 to the PTW microDiamond for a 10x10cm2 field size at a depth of 5cm.

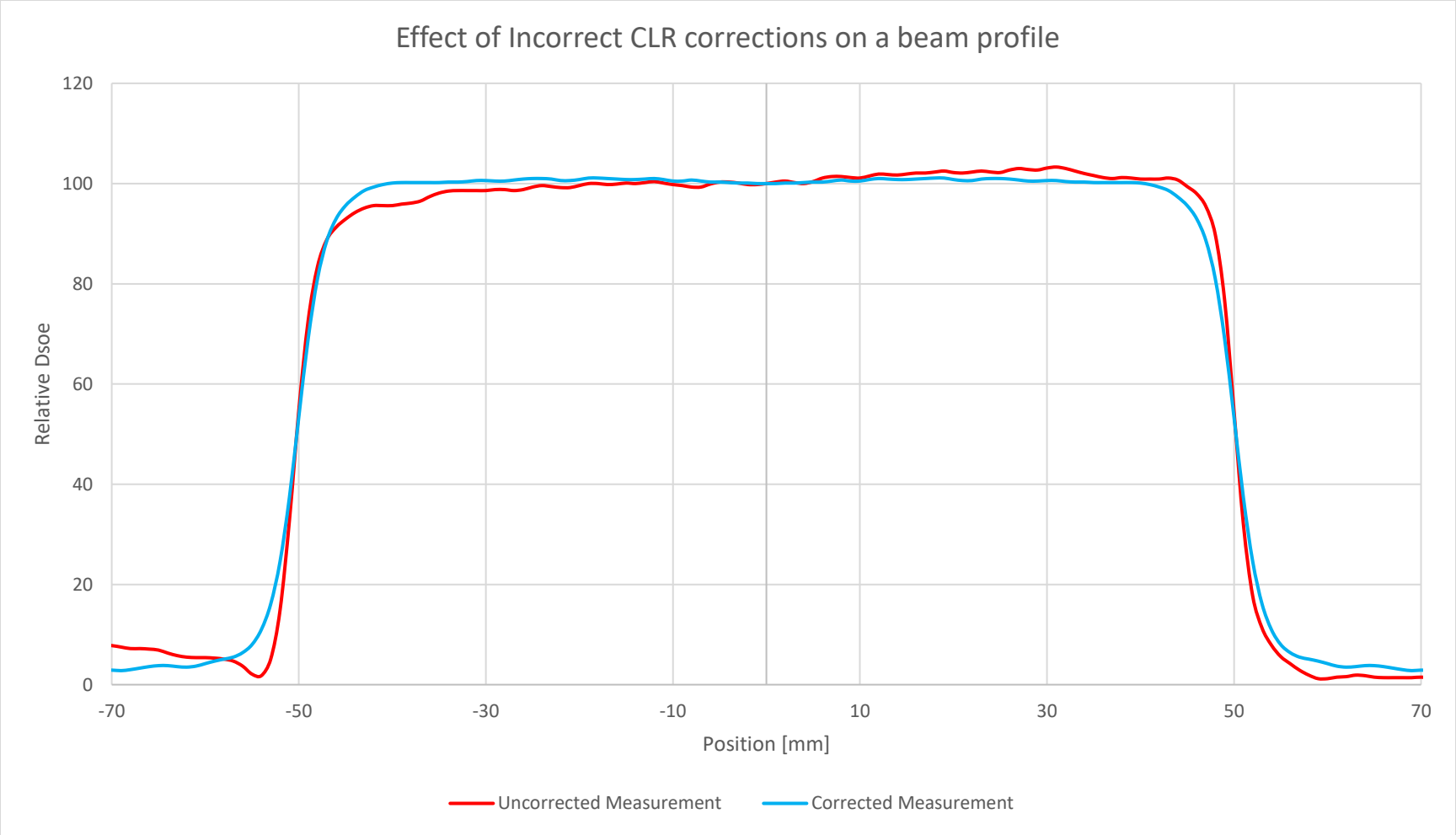

Figure 23. Example of an incorrectly calibrated profile measurement. 6MV 10x10cm2 jaw field measured at Dmax in water.